www.lpr-journal.org Vol. 7 No. 3 May 2013

LASER & PHOTONICS REVIEWS

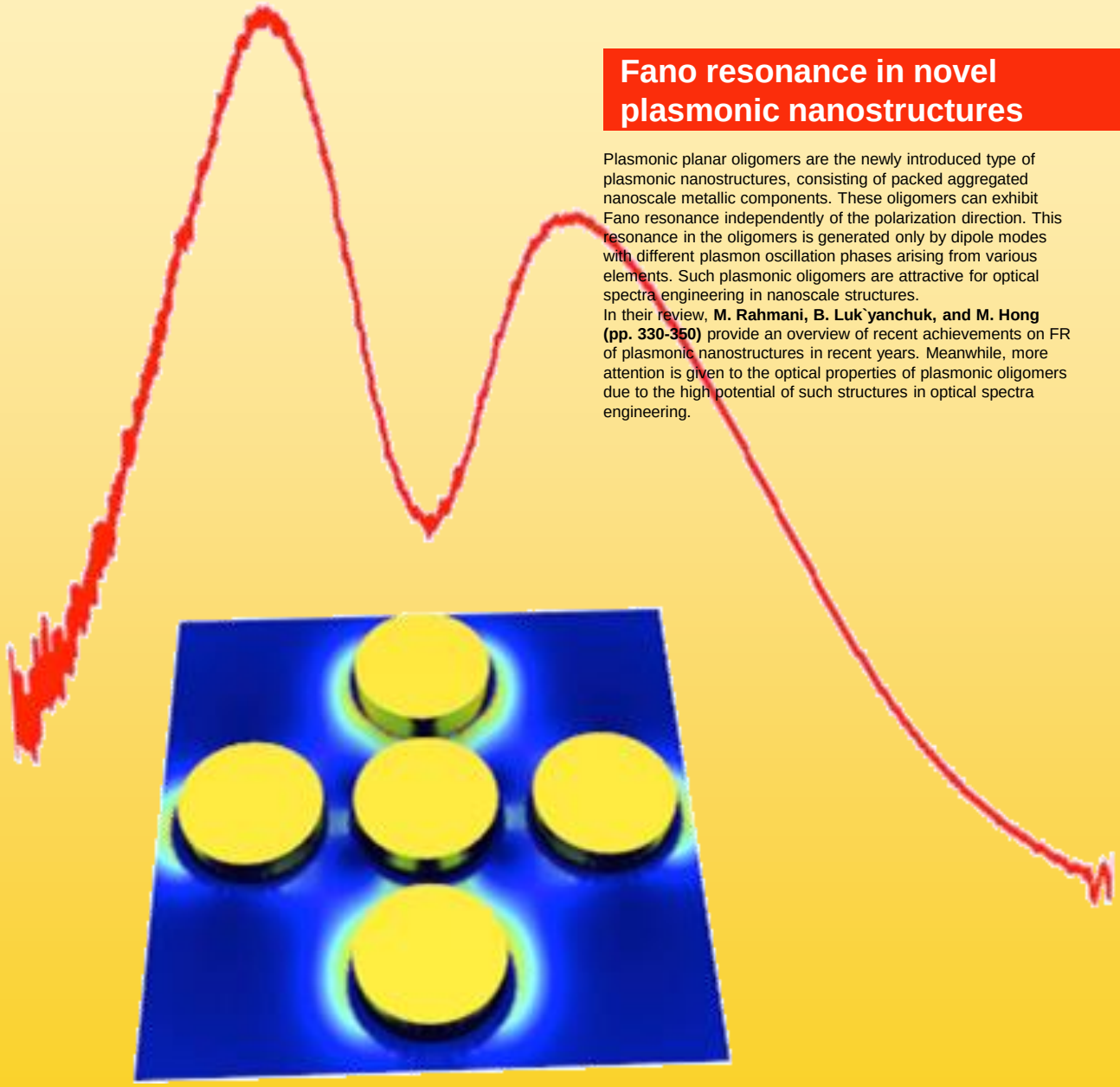

Fano resonance in novel plasmonic nanostructures

Plasmonic planar oligomers are the newly introduced type of plasmonic nanostructures, consisting of packed aggregated nanoscale metallic components. These oligomers can exhibit Fano resonance independently of the polarization direction. This resonance in the oligomers is generated only by dipole modes with different plasmon oscillation phases arising from various elements. Such plasmonic oligomers are attractive for optical spectra engineering in nanoscale structures.
In their review, **M. Rahmani, B. Luk`yanchuk, and M. Hong (pp. 330-350)** provide an overview of recent achievements on FR of plasmonic nanostructures in recent years. Meanwhile, more attention is given to the optical properties of plasmonic oligomers due to the high potential of such structures in optical spectra engineering.

WILEY-VCH

WILEY ONLINE LIBRARY

Early View publication on wileyonlinelibrary.com
(issue and page numbers not yet assigned;
citable using Digital Object Identifier – DOI)

LASER & PHOTONICS REVIEWS

Laser Photonics Rev., 1–21 (2012) / **DOI** 10.1002/lpor.201200021

Abstract Recently, a large number of experimental and theoretical works have revealed a variety of plasmonic nanostructures with the capabilities of Fano resonance (FR) generation. Among these structures, plasmonic oligomers consisting of packed metallic nanoelements with certain configurations have been of significant interest. Oligomers can exhibit FR independently of the polarization direction based on dipole–dipole antiparallel modes without the need to excite challenging high-order modes. The purpose of this review article is to provide an overview of recent achievements on FR of plasmonic nanostructures in recent years. Meanwhile, more attention is given to the optical properties of plasmonic oligomers due to the high potential of such structures in optical spectra engineering.

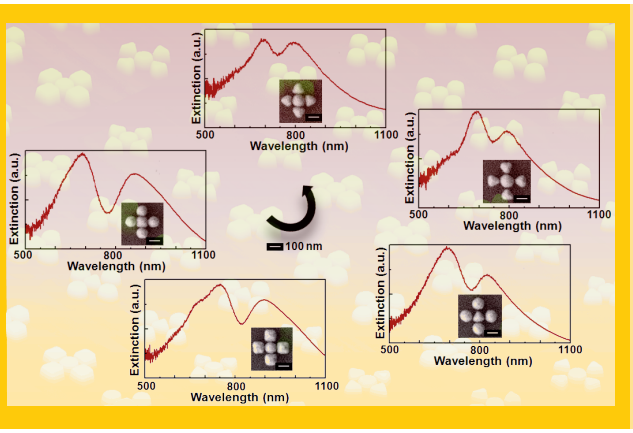

REVIEW ARTICLE

Fano resonance in novel plasmonic nanostructures

Mohsen Rahmani[1,2], Boris Luk'yanchuk[1,*], and Minghui Hong[2]

1. Introduction

Fano resonances (FRs) generation and applications have become popular in recent few years due to the large number of potential applications in the development of chemical or biological sensors, filters, lasing, switching, nonlinear and slow-light devices and electro-optics, etc. [1, 2]. Ugo Fano experimentally observed this new type of resonance in 1935 with a distinctly asymmetric shape in the absorption profile of noble gases [3] and theoretically described it in quantum autoionizing states of atoms in 1961 [4]. His understanding was based on the overlap of a discrete state with a continuum state, where destructive and constructive interferences take place at close energy positions, which results in the asymmetric profile [4]. Until the end of 20th century, this phenomenon has been studied basically for quantum systems. However, the basic interference effect in the classical system of coupling oscillators has been well known for a long time and has been used extensively in mechanical systems for dynamic damping [5]. Recently, Fano interferences have been applied successfully to explain a large number of phenomena in various systems. These phenomena include the quantum transport in quantum dots, wires and tunnel junctions [6–8], the energy-dependent line profile of absorption in molecular systems [9, 10], bilayer graphene nanostructures [11, 12] and the asymmetric distribution of the density of states in Anderson impurity systems [13] as well as several optical systems, such as strong coupling between Mie and Bragg scattering in photonic crystals [14, 15] and terahertz metamaterials [16–28].

Among all these systems, the field of plasmonics has become one of the most active platforms in FR generation and applications due to its convenience to generate the coherent effects [29–41]. It is well known that metallic nanostructures can sustain surface plasmons that are the coherent oscillations of the conduction electrons at the interface between metal and dielectric materials [35]. Since the relevant interaction parameters can be tuned by changing the geometry and composition of nanostructures, plasmonic systems have proven to be an ideal choice to generate FRs with sharp dispersion. In such systems, FR occurs via the spectral overlap of broad superradiant and sharp subradiant resonance modes, which are typically characteristics of dipolar and high-order modes, respectively. Comprehensive descriptions of fundamental Fano theory and its progress through many designs of plasmonic nanostructures can be found in recent reviews [1, 2, 42–45].

Plasmonic planar oligomers as the newly introduced type of plasmonic nanostructures, consisting of packed aggregated nanoscale metallic components, have also been investigated to exhibit FR in the visible and near-infrared ranges. These structures are of significant interest due to their fundamental importance as a model system to understand the nature of electromagnetic coupling [46–62]. Hybridization of plasmons arisen from finite number of individual elements of oligomers is found to excite multiple plasmon resonances with large induced electromagnetic field enhancement. Unlike most of the other plasmonic nanostructures in which a dark high-order mode and its overlap with a bright dipole mode is a requirement for FR to appear [1, 2, 42–45], the sharp FR in the oligomers is generated only by dipole modes with different plasmon oscillation phases arising from various elements. It can address the challenges of high-order modes excitation and make the

[1] Data Storage Institute, 5 Engineering Drive 1, Off Kent Ridge Crescent, Singapore 117608, Singapore
[2] Department of Electrical and Computer Engineering, National University of Singapore, 4 Engineering Drive 3, Singapore 117576, Singapore
[*] Corresponding author: e-mail: Boris_L@dsi.a-star.edu.sg

oligomers unique devices for biosensing. On the other hand, while the far-field optical properties of oligomers are polarization independent, the near-field energy can be flexibly redistributed inside the arbitrary interparticle gaps by changing the polarization orientation. This ability may be used for optical switching and nonlinear spectroscopy. Despite all these interesting capabilities of plasmonic oligomers, there is still lack of exploratory overview on these structures as excellent candidates in the development of optical devices. In this review paper, the main attention is given to plasmonic oligomers as multitask structures that can exhibit interesting optical properties. Meanwhile, a review is also provided on the recent newest achievements in FR generation, identification and applications in other plasmonic nanostructures since last year that are generally not covered in the aforementioned recent reviews.

2. FR generation

2.1. Symmetry breaking

In addition to extensional studies on the theoretical physics behind FR generation [63–74], a large number of papers have recently investigated how geometrical symmetry breaking [75–109] can lead to FR observation in the optical spectra. A common feature shared by these investigations is the overlap of a discrete state with a continuum state accompanied by close energy positions of the destructive and constructive interferences. In addition to the classic symmetry broken structures such as dolmen and concentric ring and disk cavities [1, 2, 42–45], it has been shown that symmetry breaking in simple structures, such as metallic nanodisks with a missing wedge-shaped slice is able to excite a FR [110, 111]. Zhang et al. have proved that in such structures, FR is a result of the coupling between a hybridized plasmon resonance of the disk and a narrower quadrupolar mode supported by the edge of the missing wedge slice. Another example of symmetry breaking is to deposit a spherical or a cubic nanoparticle on an adjacent semi-infinite dielectric [112, 113]. It has been demonstrated that the unique geometry of a perfect cube can also lead to the strong interaction and hybridization of the primitive modes of a nanocube through the underlying substrate. Subsequently, FR in this case can be explained by the substrate-mediated interaction of a dark quadrupolar cube mode with a bright dipolar cube mode [112,113]. These studies confirm that breaking and tuning the geometry of nanostructures can contribute to the generation of narrow band dark modes and its spectral overlap with broad bright modes.

2.2. Hybrid nanostructures

It has been evaluated that complex and hybrid structures [114–165] can fulfill the FR requirement for bright and dark modes hybridization as well. For instance, a simple combination of a cross-shaped structure and a nanobar can provide a clear evidence that once the energy of a dark mode approaches the energy of the bright mode, the FR can be observed as a characteristic asymmetric lineshape [166]. In such XI cavities, the coherent near-field coupling takes place between broad dipole and sharp quadrupole modes being excited in the cross, and excited dipole resonance in the bar [166]. An alternative way to generate FR is by forming nanometric apertures in metallic thin films [167–173]. Artar et al. [167] presented a method to exhibit multiple spectral optical properties by fabricating the apertures on multilayer thin films. Their proposed structure consists of two complementary metamaterial layers being separated by a small dielectric gap. This gap enables strong near-field interaction in between. Each planar layer possesses bright and dark modes to couple to each other through the structural asymmetry enabling multispectral FR behavior. In fact, the apertures in multilayer thin films can realize so-called multispectral plasmon-induced transparency.

2.3. Gratings

Coupled waveguide grating structure is another compelling approach to generate FRs [174–180]. Knowing that the grating structure exhibits waveguide resonance, Christ et al. [181] investigated the coupling between localized particle plasmons and optical waveguide modes, which leads to the appearance of a Fano signature in transmission spectra. But the coupling between narrowband waveguide resonance and other additional generated resonances, such as Fabry–Pérot (FP) microcavity resonance [174] or additional modes arising from the chains of metal bumps on slit sidewalls [164] as the contributing factor of FR generation in gratings, is still a subject of debate.

2.4. Fanoshells

One more plausible candidate to generate FR is chemically fabricated Fanoshells [182–188]. Fanoshells typically consist of a metallic core surrounded by a dielectric spacer and subsequently another metallic shell [186, 189], while the central core is usually displaced with respect to the metallic core. In these structures, FRs are induced by interaction between dipolar modes of the inner core, and multipolar plasmon modes of the outer shell. Fanoshells possess optical properties similar to so-called nanoeggs, which consist of a dielectric core surrounded by a metallic shell of nonuniform thickness [190]. Muhlig et al. [184] showed that it is possible to combine self-organization and colloidal nanochemistry methods to fabricate clusters consisting of dielectric core spheres, which are smaller than the wavelength of the incident irradiation and are decorated by a large number of metallic nanospheres. Such a core–shell system exhibits a dispersive effective permeability, i. e. artificial magnetism [185]. Meanwhile theoretical studies on ultrafast optical dynamics of excitons in nanoshell J-aggregate complexes show their potentials to enhance and tune nonlinear optical properties [182].

2.5. Mismatched nanorods

It is also worth noting that generally Fano-like responses can be obtained with mismatched dimers built from pairs of closely spaced elements [191–197]. It has been demonstrated that the FR can be obtained as simply as coupling between short and long nanorods as a result of interference between the bright mode of the short nanorod and the dark mode of the long nanorod in the dimer [63, 195–198]. This concept has been shown recently by Bozhevolnyi et al. [63] with uncoupled and detuned resonators, which were used for slow-light applications and Evlyukhin et al. [198] by golden nanorods at different lengths, which can be used for high-sensitivity monitoring of the environmental refractive index. A pair of gold and silver nanodisks with wavelength-dependent directional scattering can also be used for the same purpose. It is shown that these bimetallic dimers are able to show phase accumulation through material-dependent plasmon resonances and scattering red and blue light in opposite directions [199]. This effect arises from an asymmetric material composition causing different resonance energies of the particles and hence leading to phase shifts between the particles of the dimer. However, this combination does not require careful size optimization or use of special geometries, but the fabrication of 2D packed bimetallic structures is still challenging. One can avoid this challenge to obtain the same effect by using scatters with the same materials but different sizes [198].

2.6. Fabrication of nanostructures exhibiting FR

In the view of nanofabrication, apart from standard electron beam lithography (EBL) [200–202], some other methods in recent years have been reported with more capabilities to fulfill the required prerequisites for FR. Farrell et al. [203] have shown that FR generation may benefit from a combined nanoimprint lithographic and block copolymer self-assembled structures. They used a highly regular dewetting process of a symmetric diblock copolymer for the hierarchal formation of microdroplets and concentric nanorings. In another approach, it was shown that nanobubbles and nanodroplets can be confined either spontaneously at the suspension/substrate interface, or in the system, allowing the assembly of nanoparticles into nanoring-like structures with a flexible control of both the size and distribution [204]. Furthermore, Vogel et al. [205] reported a successful colloidal lithographic method to construct stacked nanocrescent dimer structures with a separation distance of approximately 10 nm. They used nonclose-packed colloidal monolayers as masks and obtained separated nanocrescent dimers. Template-confined dewetting [206], template-guided self-assembly [62], synthesis by seed-directed deposition [207], surfactant-assisted shape-controlled synthesis [208], DNA scaffolding [50] and assembly of gold nanoparticles in spherically confined microphase separation structures of block copolymers [209] are some recently developed fabrication methods that were used to fabricate nanostructures exhibiting FR. Laser microlens array lithography, which can realize arbitrary micrometer patterns over a large area at a high speed, is a promising method to be used in FR research, as well [210–212]. Angle-controlled colloidal nanolithography as a fast and low-cost fabrication technique [213, 214] is also one of the novel high-potential fabrication methods that will be explained in detail later in the section on oligomers.

2.7. FR in sub-10-nm structures

One important factor in the above-mentioned studies is the scaling of nanostructures exhibiting FR [215]. Most of the experimentally realized plasmonic structures have a characteristic scale of 100 nm and beyond [75–213]. It has a deep physical reason based on the Mie theory, which has been discussed in less detail. There is an intention to explain it briefly in this paper. For simplicity, we illustrate for the case of spherical nanoparticles. Within the Mie theory the lowest terms, which produce the interference necessary for FR, are related to dipole and quadrupole resonances [1,2]. When the size parameter tends to zero, these terms start from different values of dielectric permittivity $\varepsilon = -2$ for a dipole and $\varepsilon = -1.5$ for a quadrupole. As a result, the crossing of these terms can occur just at the size parameter by the order of unity (see Fig. 1a). A similar effect takes place on the hybridization diagrams for all practical nanostructures, where with the diminishing of the scale, the dipole and quadrupole resonances arise from different values of ε. It appears that FR is forbidden for nanostructures at a size parameter much smaller than unity. However, some attractive applications of FR, e. g. in data-storage technology, need the scale of structures of about 10 nm [215]. This reveals the importance of FR generation in ultrasmall structures [216]. It is found that there is some important conformance exception for struc-

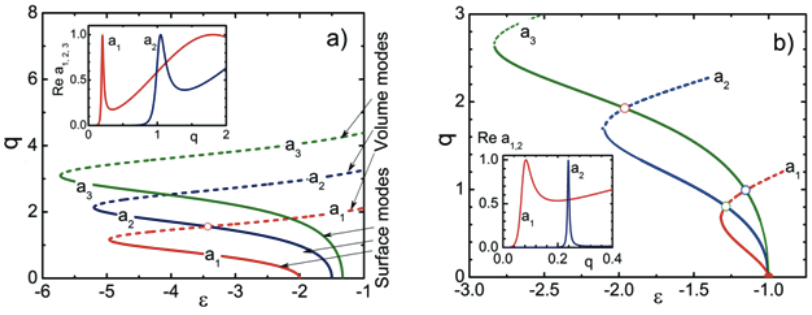

Figure 1 (online color at: www.lpr-journal.org) Trajectories of the three first optical electric resonances a_1 (dipole), a_2 (quadrupole) and a_3 (octopole). (a) refers to a sphere and (b) refers to a cylinder. The lower (solid) branches present the narrow surface plasmon modes and upper (dashed) branches present the corresponding broad resonances. The insets show the plots of dipole (red) and quadrupole resonances (blue) versus size parameter at $\varepsilon = -2.1$ (a) and $\varepsilon = -1.02$ (b).

tures with cylindrical symmetry. For such structures, all surface plasmon resonances for small-size parameters start from the same value $\varepsilon = -1$. This permits production of FR within extrasmall nanostructures at size parameters much less than unity (see Fig. 1b). This undertaking may provide very good guidelines for FR generation in ultrasmall nanostructures, which may lead to high-potential applications on the molecular scale.

2.8. FR in coupled oscillators

One shared factor among most of the addressed studies is that the dispersion of FR arises due to interference between broad and narrow spectral lines. It has been explained that the broad spectral line in nanostructures can be excited directly by incident light and permanently exists due to Rayleigh scattering. But the best method to create a narrow spectral line in the vicinity of this broad resonance is still a subject of debate due to its challenges. Although extensive research works on FR have been promised to create such narrow spectral lines by indirect excitation of dark modes in plasmonic nanostructures, we intend to present a simple proof by a classical harmonic oscillator system that even in the absence of dark modes, light is capable of exciting two different modes simultaneously equally and directly. It may lead to FR generation even with a high contrast. The analogy of FR in plasmonic systems to the classical resonances in the harmonic oscillator system has been established in various studies recently [1, 2, 72, 217, 218]. The basic feature of such systems has a manifestation as a coupled behavior of two effective oscillators associated with propagating and evanescent waves. The motion equations of oscillators $|1>$ and $|2>$ can be solved in terms of displacements $x_1$and $x_2$from the equilibrium positions:

$$\begin{aligned} \ddot{x}_1 + \gamma_1 \dot{x}_1 + \omega_1^2 x_1 - \Omega^2 x_2 &= f_1 e^{-i\omega t}, \\ \ddot{x}_2 + \gamma_2 \dot{x}_2 + \omega_2^2 x_2 - \Omega^2 x_1 &= f_2 e^{-i\omega t}. \end{aligned} \tag{1}$$

Where ω_1 and ω_2 are oscillation frequencies, corresponding to the oscillators 1 and 2, respectively, and parameter Ω describes the coupling of the oscillators. γ_1 and $\gamma_2$are the friction coefficients, which are used to account for the energy dissipation of $|1>$ and $|2>$, respectively. The steady-state solutions for the displacement of the oscillators are also harmonic: $x_1 = x_{10}e^{-i\omega t}$, $x_2 = x_{20}e^{-i\omega t}$, and corresponding amplitudes are given by

$$\begin{aligned} x_{10} &= \frac{f_2\Omega^2 + f_1\left(\omega_2^2 - \omega^2 - i\gamma_2\omega\right)}{\left(\omega_1^2 - \omega^2 - i\gamma_1\omega\right)\left(\omega_2^2 - \omega^2 - i\gamma_2\omega\right) - \Omega^4}, \\ x_{20} &= \frac{f_1\Omega^2 + f_2\left(\omega_1^2 - \omega^2 - i\gamma_1\omega\right)}{\left(\omega_1^2 - \omega^2 - i\gamma_1\omega\right)\left(\omega_2^2 - \omega^2 - i\gamma_2\omega\right) - \Omega^4}. \end{aligned} \tag{2}$$

The paradigm of the classical analog of FR is that light excites only the broad mode, e. g. x_1, while the narrow resonance mode x_2 (dark mode) is excited just due to the coupling. In this sense, only one oscillator is taken to be driven by a harmonic force where $f_2 = 0$. An example of this understanding can be seen in Fig. 2a.

But it can be examined simply that both modes can be excited directly, i. e. light equally excites both broad and narrow modes. In this case, the Fano lineshape appears even when one has not any dark mode. The plots in Fig. 2b indicate that when both oscillators are driven by harmonic forces, the resonance sharpness can be even higher. It is important for higher figure of merit (FoM) in all FR appli-

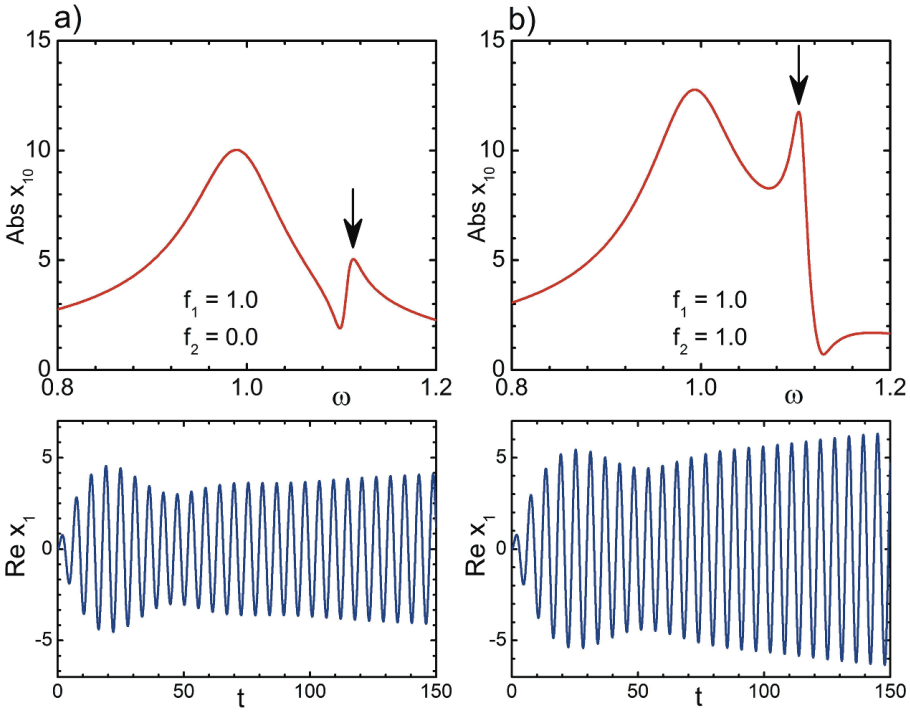

Figure 2 (online color at: www.lpr-journal.org) Amplitudes of resonances of coupling oscillators with $\omega_1 = 1$, $\omega_2 = 1.1$, $\Omega = 0.25$, $\gamma_1 = 0.1, \gamma_2 = 0.01$, $f_1 = 1$. The only difference is $f_2 = 0$ in case (a) and $f_2 = 1$ in case (b). The plots below show temporal variation of the signal at corresponding indicated resonant frequencies (shown by arrows).

cations. One should not overlook that in both cases, interference effects exist.

It is noteworthy that it is not easy to realize sharp FR with significantly different values of damping constants γ_1 and γ_2 for two coupled oscillators. However, even under condition $\gamma_2/\gamma_1 \approx 1/3$ one can see asymmetrical resonance. Na and Ag nanoclusters can be good candidates for this argument. Due to their different material properties, their damping constants γ_1 and $\gamma_2$differ from each other [219]. But nanoclusters of Na and Ag have close resonance frequencies (for dipole surface plasmon resonances: $\lambda_1 = 377$ and $\lambda_2 = 354$ nm), while their dissipation parameters differ by more than threefold: $\gamma_1 = 0.178$ and $\gamma_2 = 0.6$. It is clear that one can see a Fano resonance within the system of coupled Na and Ag particles.

3. Plasmonic planar oligomers

Oligomers are novel nanostructures in which the sharp FR excitation is based on the coupling of the antiparallel dipole modes [46–62, 220–224]. This trend is contrary to symmetry breaking or complex nanostructures in which FR is a result of the coupling between dipolar and multipolar modes. Oligomers consist of aggregating nanoelements with sufficiently small interparticle separation. The combination of the plasmon modes of each constituent nanoparticle leads to the formation of collective plasmon modes in the whole structure. Such strongly coupled particle aggregates show much higher sensitivities to structural and environmental changes as compared to uncoupled particles. This intriguing fact has stimulated several research studies. It is demonstrated that in many cases, group theory can be used to identify the microscopic nature of the plasmon resonances [47, 52, 54, 60, 61], e. g. to elucidate the effect of different element configurations on the optical properties of symmetric silver nanospheres aggregations [47].

Among the fabrication methods listed previously, electron beam lithography, colloids self-assembly, DNA scaffolding and angle-controlled colloidal nanolithography are the most often used methods to fabricate planar oligomers. Among nanolithographic planar ensemble oligomers, planar symmetric quadrumers [49,52,60], pentamers [50,52,57,58] and heptamers [46, 52, 54–56] were most widely studied recently. It has been demonstrated that the far-field optical properties of such oligomers, including its FR, are isotropic and hence independent of the orientation of the inplane polarization of the incoming light. This is a milestone of oligomers with strong capabilities for many potential applications, such as surface-enhanced spectroscopies, nanoantennas, and biochemical sensors [54]. In the oligomers, when the oscillating plasmons in all nanoparticles are in-phase, the net mode arising from the oligomers is superradiant. But the plasmons arising from various individual elements may not oscillate in phase. The signature of subradiant mode, which leads to FR existence, appears when the plasmons arising from individual elements oscillate out of phase compared to each other.

3.1. Far-field and near-field optical properties

Initially, the experimental optical properties of planar symmetric heptamers, consisting of one central and six surrounding ring-like nanoelements, were studied [51, 54, 55]. It has been demonstrated that the interference between subradiant and superradiant modes, leading to a pronounced FR in such structures, is governed by the presence of the central element [54, 55]. The resulting FR is attributed to the hybridization of the plasmons in the central nanoparticle and the ring-like hexamer. In the superradiant mode, all seven clusters oscillate in phase, leading to significant spectral broadening due to strong radiative damping. The subradiant mode is characterized by an out-of-phase oscillation of the net dipole moment of the dipolar plasmon modes of the inner particle and the outer ring. They ideally can cancel each other completely and render the subradiant mode. Therefore, by removing the central particle, one can switch on and off the FR without a need for the symmetry breaking. Furthermore, the interparticle separation plays a curial role in the formation of the collective modes as it determines the coupling strength between the constitutes of the heptamer [54]. Small interparticle gaps result in a strong FR for the compact heptamer. This pronounced FR can be seen in the measured extinction (1 – transmission) spectrum at a wavelength of $\sim$ 800 nm for the plasmonic heptamer in the top of Fig. 3a. In this case, disk diameters and interparticle gaps are 140 nm and 20 nm, respectively. Isotropic far-field optical properties of symmetric heptamers can be seen clearly via similarity of extinction spectra at both x- and y-polarized incident light. A detailed study on the effect of heptamer component size, geometry and interparticle gap can be found in Refs. [54, 55].

The role of individual nanoparticles in the collective behavior of plasmonic oligomers has also been studied [52]. As can be seen in the middle and bottom spectra of Fig. 3a, gradually varying the size of one satellite nanoparticle gives rise to the drastic reduction of the structural symmetry. The undisturbed heptamer belongs to the symmetry group D_{6h} (C_{6v} if the substrate is considered), whereas the defective heptamer is of $D_{1h} = C_{2v}$ symmetry ($C_{1v} = C_{1h} = C_s$ if considering the substrate). Although the optical properties of defective heptamers are no longer isotropic, such structures still have one symmetry axis, which is along the center and the defect particles. Figure 3a shows that decreasing the size of one satellite nanoparticle suppresses the superradiant profile line widths for both TM and TE polarizations. Simultaneously, a blueshift of the FR can be observed. The magnitude of this energetically shift strongly depends on the orientation of the polarization of the incoming irradiation with respect to the defective nanoparticle [52].

It was also shown that breaking the symmetry of the heptamer by displacing the central particle from its center position enables intriguing resonant behaviors. The formation of a true defect by physically bridging the center particle and one ring particle leads to the formation of dumbbell-like structures. Figure 3b shows the onset of strong dipolar resonance excitable along the dumbbell-shaped structure. In this case, the neighboring isolated particles mostly oscillate in

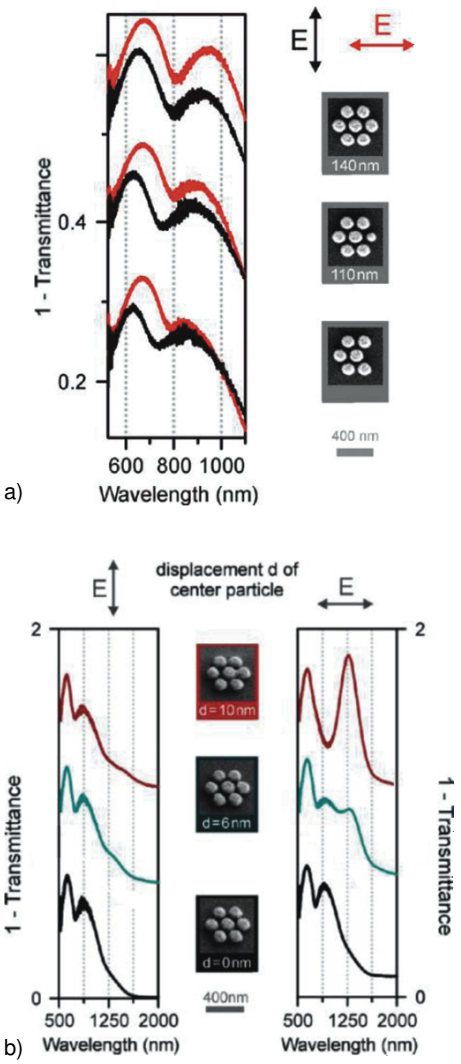

Figure 3 (online color at: www.lpr-journal.org) (a) Right: Normal-view SEM images of the corresponding structures with indicated defect particle sizes. Left: Experimental extinction spectra of the defective heptamer structures in dependence on the defect particle. (b) Experimental extinction spectra of the plasmonic heptamer structures in dependence on the lateral displacement of the center nanoparticle to the right for vertical (left column) and horizontal (right column) polarizations. The nominal displacement d of the middle particle from its center position is given below the corresponding SEM images (middle column). The scale bar is 400 nm. (Adapted with permission from two figures of [52], © 2011, American Chemical Society.)

phase and the spectral response is dominated by the dipolar plasmons in the dumbbell-like particle. FR is subsequently carried out by this long-wavelength mode and vanishes completely. Strikingly, for excitation perpendicular to the defect, the FR is nearly undisturbed. Meanwhile, symmetry lowering of FRs by applying a uniaxial mechanical stress to heptamers being fabricated on a flexible polydimethylsiloxane membrane [221] and a remarkable redshift of the FR with increasing refractive index of the surrounding medium are other highly promising research studies [55].

It is noteworthy that the subradiant and superradiant modes have substantially different linewidths, as manifested in the spectra of the clusters. Both modes suffer from intrinsic losses and dephasing, such as Drude damping. In the ideal case, the subradiant mode does not decay radiatively as it does not possess a net dipole moment. Thus, the dephasing of the lifetime of the subradiant mode is strongly prolonged, explaining the highly enhanced local near-field associated with it. Ye et al. [224] have recently shown that geometry parameters of heptamers can be used to modify the near-field properties of FR. They established surface-enhanced Raman scattering (SERS) measurements of a para-mercaptoaniline (p-MA) monolayer adsorbed on structures. They used the obtained maps to provide a physical picture of near-field localized energy in heptamers and finally integrated it over the surface of the heptamers to find relative enhancement factor for each cluster. Figure 4 shows the effect of interparticle spacing on the scattering spectra and SERS response of a heptamers. Figure 4a shows the SEM images of a heptamers with 130-nm diameter disks and gap sizes of 15 nm (i), 20 nm (ii), 30 (iii), and 60 nm (iv). The dark-field experimental and simulated scattering spectra shown in Figs. 4b and c reveal that the Fano dip of the heptamer (functionalized with p-MA molecules) weakens and blueshifts when the gap size increases. The corresponding Raman spectra are shown in Fig. 4d. It can be seen that the Stokes modes that appear at 1080 and 1590 cm^{-1} indicated by blue and pink arrows, respectively, reach maximum intensities for the heptamer with the smallest 15 nm gap size (i), decreasing significantly for a slightly larger gap size at 20 nm (ii), and disappearing almost entirely for the elements at the larger gap sizes of 30 and 60 nm (iii and iv, respectively). The SERS maps show that when the gap size increases, the SERS hot spots between the top/bottom two disks are the first to diminish as compared to the hot spots in the gaps between the central and side disks. This reveals its capability to detune the FR from the pump and Stokes wavelengths with a resulting decrease in SERS signal [224].

Furthermore, Alonso-Gonzalez et al. [46] used interferometric near-field microscopy to image the interference responsible for FRs. However, mapping the electron beam excited full plasmonic mode in nanocavities by the electron energy-loss spectroscopy [225] and cathodoluminescence [226–228] techniques have also been presented, but Alonso-Gonzalez et al. [46] reported a dramatic redistribution of the electric-field intensity and phase across the structure around FR. Their real-space near-field imaging provides a detail verification of interfering plasmonic modes and their coupling. It can also be observed by a new method of quantitative phase measurement, presented by Carney et al. [229].

Frimmer et al. [230] also showed that cathodoluminescence (CL) can be used to reveal the optical properties of oligomers. They showed an enhancement in the radiative local density of optical states at the same wavelength of a Fano feature in the extinction spectra of heptamer. Meanwhile, Lassiter et al. [231] performed wavelength-selected cathodoluminescence spectroscopy and imaging in nonamers and demonstrated that a deconstruction of the Fano lineshape

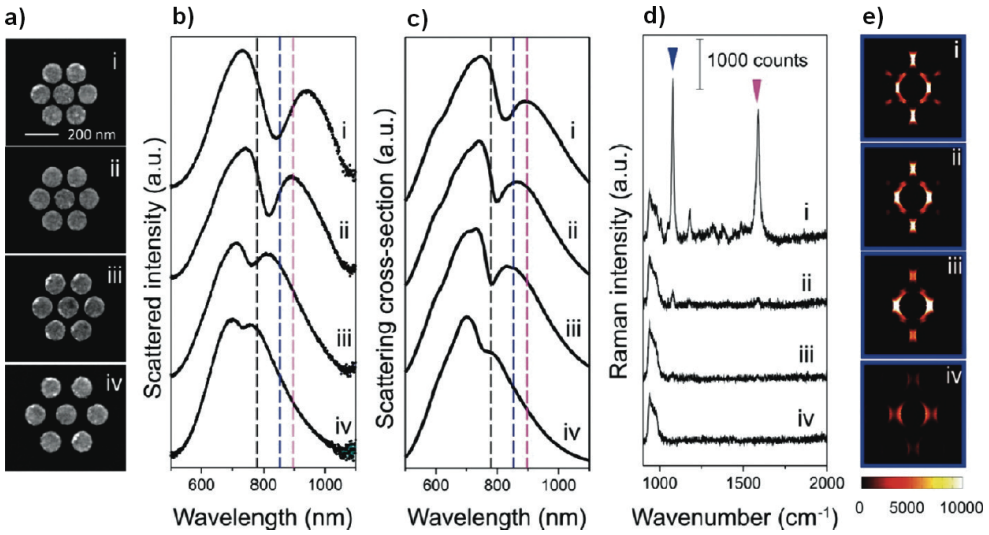

Figure 4 (online color at: www.lpr-journal.org) Scattering spectra and SERS properties of individual Au heptamers with varying gap sizes: (i) ∼15 nm, (ii) ∼20 nm, (iii) ∼30 nm, and (iv) ∼60 nm gaps. In all cases, the height of the disks is 30 nm and the diameter of the disks is 130 nm. (a) SEM images, (b) experimentally obtained dark-field scattering spectra, (c) calculated scattering spectra (FDTD), and (d) SERS spectra of a monolayer of p-MA molecules on individual heptamers (i-iv) with horizontal incident polarization. The black dashed lines in (b, c) show the excitation laser at 785 nm; blue and pink dashed lines show the Raman Stokes lines of p-MA molecules at 1080 and 1590 cm^{-1} (indicated by the blue and pink arrows in (d)), respectively. (E) SERS maps for the 1080 cm^{-1} Stokes mode of p-MA on heptamers (i-iv) evaluated at one-half the height of the structure. (Adapted with permission from [224], © 2012, American Chemical Society.)

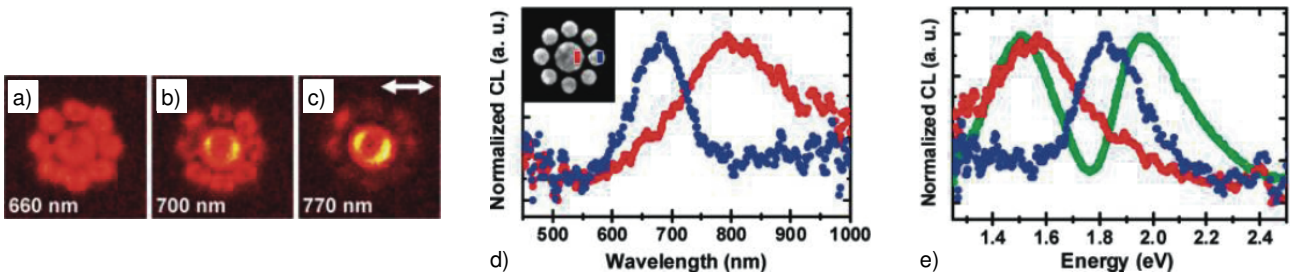

Figure 5 (online color at: www.lpr-journal.org) Polarized wavelength-selected cathodoluminescence images of a nonamer at (a) 660, (b) 700, and (c) 770 nm. Arrow indicates analyzer angle. (d) Cathodoluminescence spectra where the electron beam is exciting the center particle (red) and a particle in the outer ring (blue). The inset shows an SEM image of a nonamer with blue and red squares to indicate the location of the beam for the blue and red spectra, respectively. (e) Experimental spectra of the plasmonic nonamer plotted in energy units: plane-wave excitation (green), excitation by electron beam impinging on an outer particle (blue), and the center particle (red). (Adapted with permission from two figures of [231], © 2011, American Chemical Society.)

arising from oligomers is possible. They moved across the FR from shorter to longer wavelengths. Figures 5a–c show wavelength-selected CL at selected wavelengths of 660, 700, and 770 nm, respectively. These plots show clearly that the contribution of the particles in the outer ring diminishes while the contribution from the central particle increases dramatically. CL spectroscopy results shown in Fig. 5d reveals that under electron beam excitation there are actually two independent resonances associated with either the center particle or the outer ring. Figure 5e shows the dark-field scattering spectrum of the nonamer, obtained with optical excitation, possess very good crossover with two CL spectra. It can be seen that crossover between two CL resonances is located at the same spectral position as the FR dip in the dark-field case [231].

3.2. Modulation of antiparallel modes and near-field localization

Later, it was found that a reduction in the number of surrounding disks leads to redistribution of antiparallel and parallel dipole modes in pentamers consisting of 4 satellite elements [57]. Since the formation of the distinct Fano-like shape in the spectrum is due to the destructive interference arising from these dipolar modes, the contrast of the FR in the heptamers is lower than the pentamers [57]. Figure 6a shows 3D AFM image of designed and fabricated pentamers. Figure 6b shows simulated (top) and measured (bottom) extinction spectra of the pentamers. As can be seen in the charge-distribution plot corresponding to the dip position of extinction spectra in the pentamers, the destructive inter-

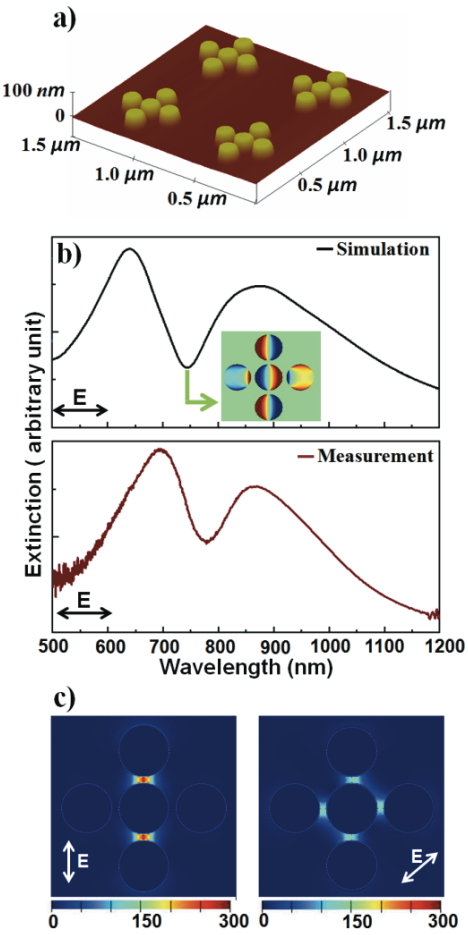

Figure 6 (online color at: www.lpr-journal.org) (a) 3D AFM image of pentamers, (b) simulated (top) and measured (bottom) extinction spectra of the pentamers for x-polarized incident light. Calculated field distribution within the pentamer at the indicated polarization directions at a wavelength of 880 nm.

ference is a result of the antiphase oscillation between the plasmons arising from three middle disks versus the plasmon of two other disks at the bottom and top. This behavior is different from the heptamer in which the destructive interference occurs when the plasmons of the six outer disks oscillate oppositely with plasmons arising from the central nanodisk.

Meanwhile, since the satellite surrounding elements of pentamers are sufficiently far from each other, they do not interact with one another. Therefore, the near-field energy in such structures takes place only between the surrounding disks and the central one. This characteristic of the pentamers provides the opportunity to tune the near-field localization known as hot spots in the arbitrary gaps. This localization can be flexibly tuned by changing the excitation polarization, while the collective far-field optical response, such as FR, is polarization independent. This tunability is obtained at a normal incidence with of a single light source rather than by coillumination with two light sources at different incident angles or with respective phase shifts [98, 232]. Figure 6c shows the near-field energy localization in the pentamers under y-polarized and 45 degree-polarized (in the X-Y plane) illumination, respectively, at the wavelength of 880 nm. It is the end point of destructive interference among plasmons arising from individual elements. From this wavelength all plasmons continue to oscillate in phase again [57]. These plots demonstrate that the field can be strongly localized in the top and bottom gaps under y-polarized excitation and in four gaps under a 45-degree polarization. These field intensities show a hundreds-fold increase inside the gaps, revealing that these separated disks can be used as an optical antenna. It is the unique feature of the pentamers to store light energy in different positions selectively by changing the polarization. This can lead to various applications in optical switching and nonlinear spectroscopy.

3.3. Hybrid oligomers

Understanding the nature of the spectral response in nanoclusters is a key point for intuitive design of the resonance lineshape characterized by its linewidth and spectral contrast that is crucial for many potential applications, such as slowing light and biosensing. Recently, it has been shown that a flexible control over the Fano profile can easily but significantly tailor the overall spectral profile in oligomers by selectively altering the particle shape without a need to change the particle size, interparticle distance or the number of elements of the oligomers [223]. This is achieved through decomposing the whole spectrum into two separate contributions from subgroups, which are efficiently excited at their spectral peak positions. Variation in particle shape of either subgroup results in the tuning of the overall spectral lineshape, which opens up a novel pathway to shape the plasmonic response in oligomers. Remarkably in the particularly considered systems, such subgroups are not due to the superposition of a subradiant and a superradiant state as described in [231], but they are the real eigenstates of the subgroups whose interference gives rise to the resonance lineshape.

Figure 7a shows simulated excitation spectra belonging to the whole pentamer as well as different potential subgroups. In addition, simply summed spectra of some of these groups illustrate clearly the essence of the interference existence in order to have a FR profile. This plot shows that if all the identified modes do not have any interference, the dip position never takes place in extinction spectra. A useful clue is that the two dominant peaks in Fig. 7a seem to be well described by two separate resonances given by the two subgroups that are illustrated in Fig. 7b. This intuition is further confirmed by calculating the electric-field intensity distribution in the pentamer at the two peak wavelengths. The field-intensity distribution plots shown in Fig. 7c clearly demonstrate that at the first peak position, the four outer disks are efficiently excited to induce strong field enhancements around each particle, while the center disk is relatively dark. Such a selective excitation of different particles is even more pronounced at the second peak position where the middle three disks become dominant, leaving the bottom and top ones completely dark. On the basis of these observations,

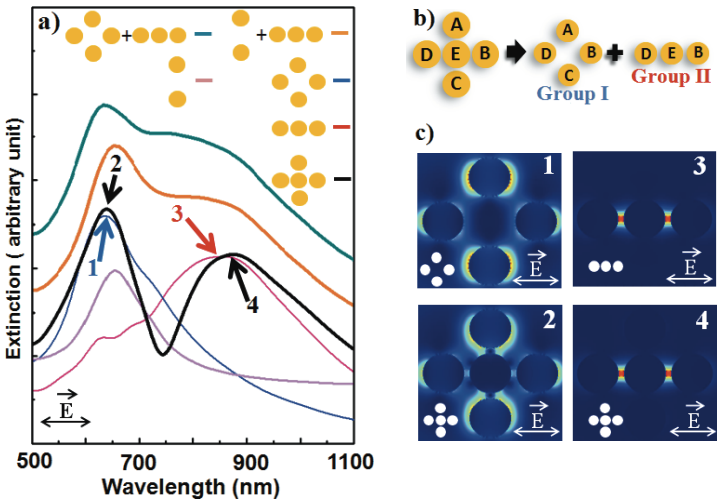

Figure 7 (online color at: www.lpr-journal.org) (a) Simulated extinction spectra of an individual pentamer (black and pink curves) and some potential subgroups and the sum of some decomposed elements. (b) Sketch of decomposing a pentamer into Groups I and II. (c) Electric-field intensity distribution in the pentamer at peaks and in the two subgroups at their respective extinction peaks. (Adapted with permission from [223], © 2012, American Chemical Society.)

it has been proposed that the complex optical excitation in the whole pentamer structure can be decomposed into two separate contributions from its subgroups, Groups I & II (see Fig. 7b). It is worthy of note that the modes that give rise to each peak in the extinction spectra are not necessarily the same as the modes that couple out of phase with respect to each other and contribute to the dip position shown in Fig. 6b.

This understanding is highly helpful to design and modify the resonance lineshape as shown in Fig. 8. Having the pentamer decomposition of Fig. 7 as a starting point, we can, for example, change the central particle shape and in

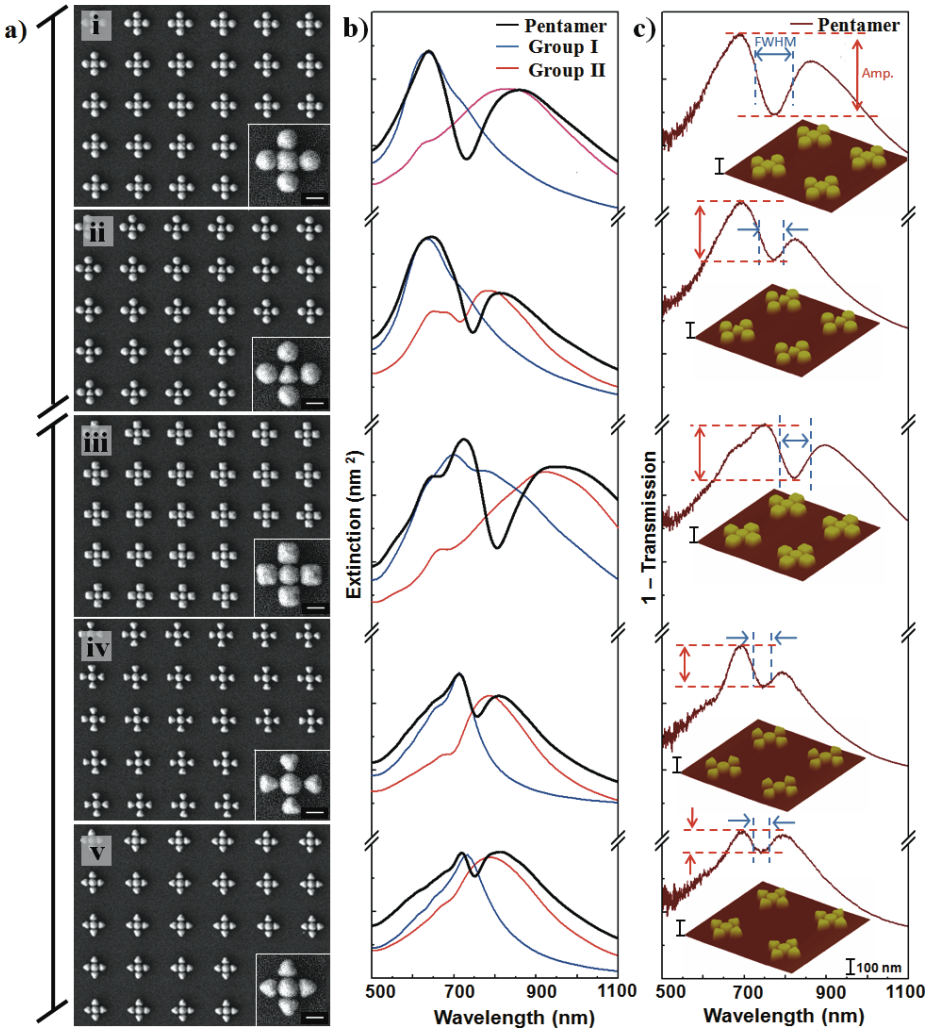

Figure 8 (online color at: www.lpr-journal.org) Tuning of resonance linewidth and spectral contrast of plasmon resonances in different pentamers. (a) SEM images of hybrid pentamers consisting of differently shaped elements. The scale bar in each image is 100 nm. (b) Simulated extinction spectra for the pentamers (black curve) and their two subgroups (blue and red curves). (c) Measured extinction spectra for the same pentamers at normal incidence, along with 3D AFM images of the nanostructures. (Reprinted with permission from [223], © 2012, American Chemical Society.)

this way we modify only the optical property of Group II, that is, only the second resonance (red curve Fig. 7a) but leaving the first one unmodified (blue curve Fig. 7a). Also as another change, for example, only the external nanoparticles, modifying Group I in this way. As can be seen in Fig. 8, by changing the shape of the nanoparticle but leaving the particle size and interparticle distance as constants, a flexible remodeling of the overall spectral shape is obtained, manifested by a systematic variation in the relative height of the two peaks as well as the resonance linewidth of the spectral dip [223].

3.4. Multi-FRs

Plasmonic oligomers have been shown as a good platform to excite multiple subradiant modes, as well. It can result in the exhibition of multiple FRs due to the interference of one superradiant and several subradiant modes. It opens up the pathway to "plasmonic supermolecules" that show unprecedented tunability, which renders them highly suitable for applications such as multiwavelength surface-enhanced Raman scattering [48]. Symmetry-broken pentamers are one of the candidates to exhibit such characteristics. The influence of symmetry breaking in the pentamers can be demonstrated by applying an offset to the central disk in pentamers [58]. Additional FR occurs while the first FR remains visible. Figure 9a shows a SEM image of designed and fabricated asymmetric pentamers with an offset in the central disk position. The smaller gap between the central disk and the nearest-neighbor disk is controlled at 3 nm. The resulting distinct FR can be observed in the simulated extinction spectrum (red line) in Fig. 9b around 2.1 eV, which is the additional FR next to the main one at around 1.8 eV. A detailed study in [58] shows that this symmetry breaking guides the structure to exhibit characteristics similar to the quadrumer proposed in [49] around 2.1 eV.

Meanwhile, it has been shown that an analogy of the optical responses to the mass–spring model is another way to prove the existence of the second FR in plasmonic systems. Figure 9b shows the comparison between two extinction spectra. Red curve represents the extinction spectrum of the indicated asymmetric pentamer, simulated by Lumerical software based on Finite- difference time-domain (FDTD) method at x-polarized normal incidence. Meanwhile black curve shows the power dissipation of the oscillator system calculated by the motion equations of a four coupled interacting oscillators model. In the coupled oscillators model, the motion equations of the oscillators are solved in terms of mass displacement from the equilibrium positions. It is a simplified model of the spring–mass model consisting of five coupled interacting oscillators in the x-direction [58]. This is due to similar coupling among the top and bottom disks with respect to the central disk that allows removing one of the masses. Thus, in this system, 3 blue oscillators represent 4 outer disks in analogous asymmetric pentamers and the red oscillator represents the central disk. Since the surrounding disks are responsible for superradiant mode exhibition in such optical systems, all blue oscillators are driven by the harmonic force $\mathbf{F}(t)$ [58]. The good agreement between the mass–spring calculated and FDTD simulated extinction spectra shown in Fig. 9b demonstrates clearly that the hybridized plasmon modes lead to the twin FRs appearance in both systems.

Higher-order FR in large oligomers have also been studied recently [48]. It was found that an added second outer ring of particles leads to plasmonic supermolecules that support additional or modified modes. Specifically, a second occurring resonance and the corresponding second-order subradiant mode could be identified. The near-field distribution indicates an antiphase oscillation of the two ring modes and the center particle. Figure 10 shows that with increasing number of particles in the clusters from $N = 7$ to 13 and 19, the overall dipole moment of the superradiant mode increases. This leads to an increased radiative damping and subsequently a spectral broadening. As can be seen in the experimental spectra in the left panel, only one Fano dip can be observed in the spectra. The FR (indicated black arrow) gradually shifts to lower energies for the larger clusters. The right panel depicts simulated spectra and clearly shows the fundamental Fano dips as well as a second FR that presents for the $N = 13$ and $N = 19$ clusters indicated by red arrows. This FR is a result of interference between the second blueshifted subradiant mode and the broad superradiant mode. It is worth mentioning that the low modulation depth of this resonance hampers its experimental observation. Only a slight kink is visible in the experiment [48].

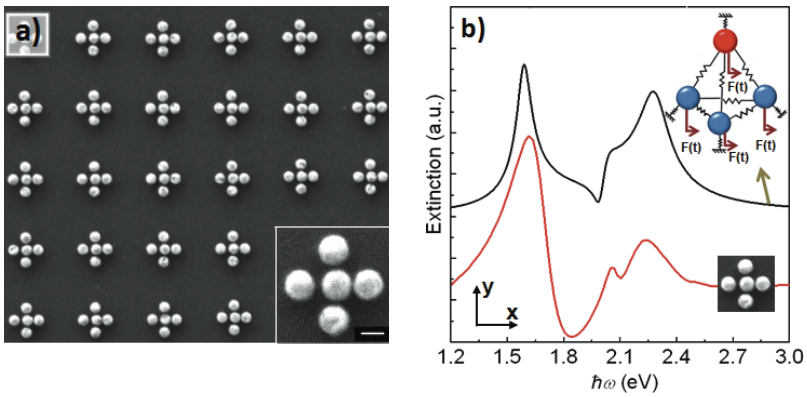

Figure 9 (online color at: www.lpr-journal.org) SEM image of the periodic array of asymmetric pentamers with an offset of the central disk leading to a corresponding gap of 3 nm. (b) Simulated FDTD (red line) and oscillator model calculated (black line) extinction spectra of the corresponding pentamer (Adapted from two figures of [58].)

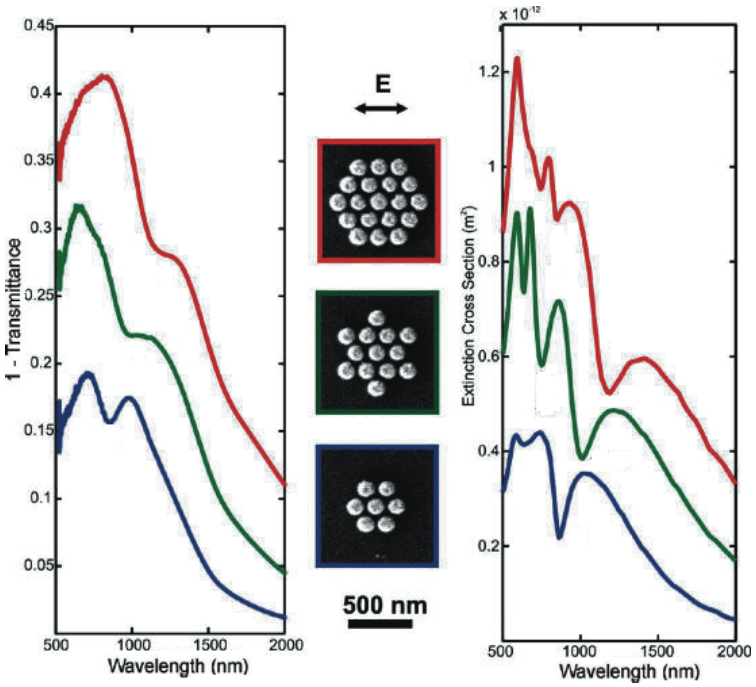

Figure 10 (online color at: www.lpr-journal.org) Experimental (1 – transmittance) spectra (left panel) and simulated extinction spectra (right panel) of the clusters (green and red curves) compared to the spectra of a heptamer (blue curves). (Adapted with permission from [48], ©2011, American Chemical Society.)

3.5. Novel fabrication methods to synthesize oligomers

Because of the high sensitivity of oligomers to the configuration of components and interparticle gaps, only certain fabrication methods can be used to synthesize such structures. Apart from EBL, colloidal self-assembly is another widely used approach in the fabrication of the oligomers. Recently, it has been shown that self-assembled nanoclusters composed of metal–dielectric spheres are possible on allowing for a precise control of the number and position of spheres in these close-packed clusters [51]. It was shown that a dielectric spacer can be used to tailor the interparticle distance between the particles down to ~ 2 nm, allowing for the observation of strong FR in these clusters. The colloidal self-assembly holds great promise in the fabrication of even more complex two- and three-dimensional structures for new types of metamaterials [51, 233]. Self-assembled quadrumers are one of well-studied oligomers that are fabricated by this method [49, 234, 235]. It was demonstrated that the asymmetric quadrumer nanoshells exhibit a pronounced FR, while the strength of this resonance strongly depends on the polarization of incident electric field due to orientation-dependent capacitive coupling within the cluster. One should note that the existence of the subradiant and superradiant modes as eigenmodes originates from the symmetry of the quadrumer geometry and can be observed in the systems of spherical particles, such as solid spheres and hollow shells [49]. In a similar study, investigation on self-assembled trimeric silver nanospehers [234] reveal that symmetry breaking can be induced by gradual opening of the vertex angle. The evaluated plasmon modes across different symmetry groups were monitored through the optical properties of the symmetry-broken trimmers. Furthermore, Yan et al. [62] used template-guided self-assembly to construct oligomers consisting of closely packed gold nanoparticles. They fabricated a few types of oligomers consisting of less than seven elements and were able to observe FRs in such systems as well.

Another promising and highly tunable approach is based on the DNA scaffolding method [236] that was used to assemble oligomers, such as heteropentamers. Such structures are another type of oligomers that exhibits pronounced FR. Assembly of DNA-functionalized nanoparticles is applied to conjugate a smaller gold sphere surrounded by a ring of four larger spheres. In this solution-based method DNAs strands were selectively assembled into the clusters in solution and act as a spacer between the conductive nanoparticles [50].

One important remark is that the characterization and subsequently applications of these methods suffer from drawbacks related to their fabrication, such as small areas in classic top-down techniques or nonrepeatability related to large-area bottom-up techniques. Recently, a novel fabrication method was introduced to tackle these limitations. It is angle-controlled colloidal nanolithography as a fast and low-cost fabrication technique [213]. Giessen and coworkers [237] have recently used this method to fabricate symmetric pentamers. As shown in Fig. 11a, the substrate is placed on a face-down sample holder that can be tilted by an azimuthal angle θ. Using another stepping motor, the sample holder can be rotated at an angle φaround the polar plane. Additionally, a programmable shutter was used between the crucible and the sample in order to further control the deposition process, which allows the preparation of complex structures consisting of different elementary shapes and even materials. During the evaporation process, the metal vapor beam passes through the apertures of the polystyrene monolayer and creates different structures on the substrate depending on the evaporation parameters, as shown in Fig. 11b. After the evaporation, the nanosphere

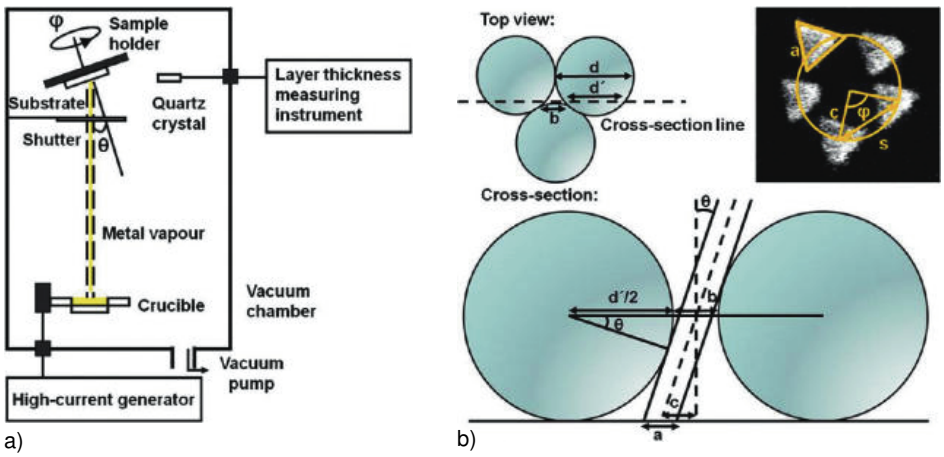

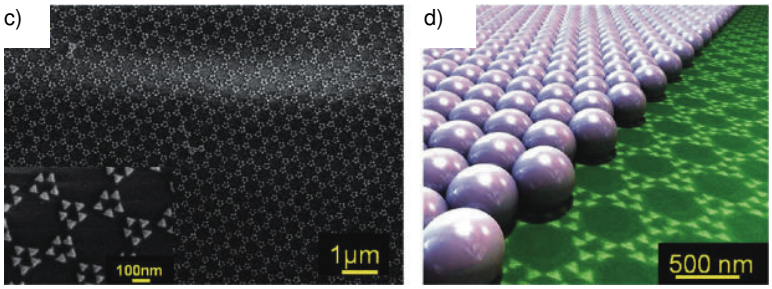

Figure 11 (online color at: www.lpr-journal.org) (a) Schematic diagram of the defined evaporation setup. (b) Simplified geometrical model for symmetric pentamer fabrication. Top left: top view. Bottom: side view at the cross section line as indicated in top view. Top right: geometrical parameters. (c) SEM images of the large area symmetric pentamers. The gap size is as small as 20 nm. (d) Artistic view of the fabrication scheme, using a real SEM image of a symmetric pentamer. (Reprinted with permission from [237], ©2011, American Chemical Society.)

mask is removed with adhesive tapes. Figure 11c shows the SEM images of the fabricated structures over a large area with excellent homogeneity and virtually no defects. Each triangular element is obtained under each aperture of the nanosphere mask at a certain angular position of substrate. Figure 11d shows an artistic impression of the fabrication process in the case of symmetric pentamers with fine gaps. Beyond the fabrication of such oligomers, this method has high potential to provide a reliable platform to generate large-area periodic plasmonic structures with complex shapes and tunable geometry parameters.

3.6. Analogy to molecular configurations

One advantage of the densely packed arrangement of metallic nanoparticles is that such structures can be regarded as highly tunable artificial molecules [238]. It is well known that the near-field associated with plasmonic resonance of the individual particles extends some distance away from it. Closely packed nanoparticles interact with each another, mediated by this near-field. This interaction is in direct analogy to molecular physics and the formation of molecules due to overlap and interaction of the electronic orbitals of the individual atoms rather than plasmonic near-field [54, 60, 239]. The qualitative basis for unraveling the energy levels of the molecular orbitals in conjugated hydrocarbon molecules in benzene is one of well-studied analogies by plasmonic oligomers [54, 239]. Similarly, in analogy to a benzene molecule, the structure of the plasmonic hexamer consisting of 6 ring-type nanoparticles [54] was used. This belongs to the D_{6h} point group, which exhibits a high spatial symmetry and the collective modes with finite inplane dipole moments belong to the E_{1u} irreducible representation. As was demonstrated earlier, a remarkable change of its resonant behavior can be seen when a central nanoparticle is introduced. This capability encourages researchers to predict the characteristics of corresponding molecules with the same configurations.

Planar oligomers consisting of a central element have a disadvantage that prevents having proper analogs to conjugated atoms in multigonal molecules. The fact is that such plasmonic oligomers are coplanar, while multigonal molecules are typically noncoplanar [60]. This is due to the tendency of the surrounding atoms to achieve the maximum distance with respect to each other under a 3D configuration so as to provide the lowest energy for molecules in the stable state. CH_4 and PCl_5 are good examples of pentagonal and hexagonal molecules, in which the central atom and the surrounding atoms are not placed in the same plane. But trigonal planar molecules, such as BF_3, SO_3 and BCl_3 possess coplanar central and surrounding atoms. Therefore, plasmonic quadrumers consisting of three similar nanodisks belonging to the D_{3h} point group are perfect candidates for analogy to trigonal planar molecules [52, 53, 60]. In fact, plasmonic quadrumers with proper disk sizes and interparticle gaps exhibit isotropic pronounced FR. Figure 12a shows the 3D AFM image of designed and fabricated quadrumers for this purpose. Since the geometrical configuration of quadrumers is the same as planar trigonal molecules, nanodisks can play the roles of artificial atoms to study the coupling trends among them. It is shown that the electronic states in trigonal planar molecules that can be predicted by the plasmon behaviors of metallic nanostructures, can

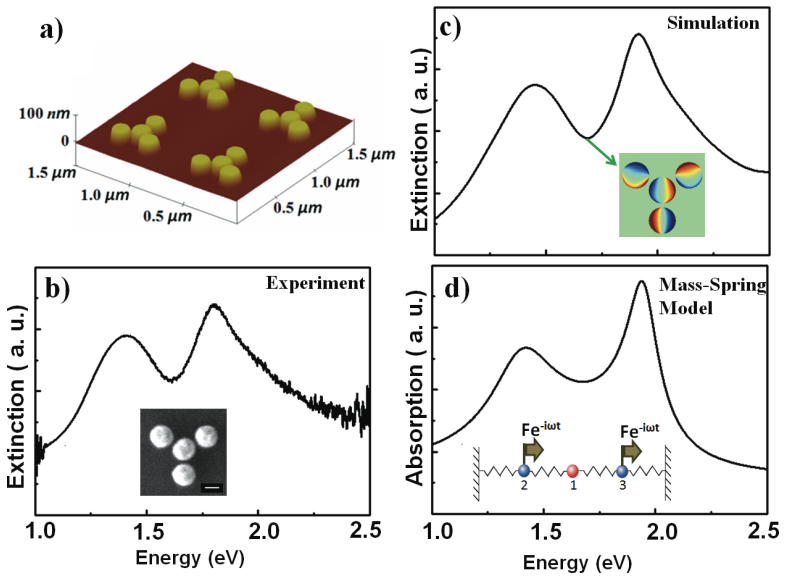

Figure 12 (online color at: www.lpr-journal.org) (a) 3D AFM images of quadrumers. (b) Measured and (c) simulated extinction spectra of the quadrumers at x-polarized normal incidence and (d) analogous absorption spectral response of mechanical mass–spring model.

be modeled with mechanical coupled oscillators as well. Figures 12b–d show the experimental extinction response, simulated spectrum and spectral absorption response of a corresponding simplified mass–spring model [60] with high agreement. These analogies of oligomers can assist the understanding of the plasmonic behaviors in nanostructures, atomic and molecular wave functions.

As another example for analogy among planar plasmonics and biochemical molecules, Liu et al. [239] examined the magnetic plasmons of fused ring structures consisting of multiple connected heptamer units. They found that in a two-unit heptamer structure, the magnetic mode consists of two opposite current loops, which leads to the emergence of an antiphase behavior of the magnetic plasmons. The plasmon supported by this structure can be regarded as the plasmonic analogy to a naphthalene molecule. The overall shape of the extinction spectrum shown in Fig. 13 is determined by a broad superradiant mode in which the charges in all of the nanoparticles oscillate inphase. The first subradiant resonance is at 1100 nm where the charges in the two center particles oscillate antiphase relative to those in the surrounding particles. The second subradiant mode at 1550 nm is characterized by ring currents circulating in opposite directions around the two fused rings with the two shared gold nanoparticles, which function as a mutual current link. The magnetic field plot at Resonance II in this figure explicitly shows the excitation of two antiparallel magnetic dipole moments in the plasmonic naphthalene structure.

These analogs open up a way to design different combinations and arrangements of oligomers [240–242]. This can

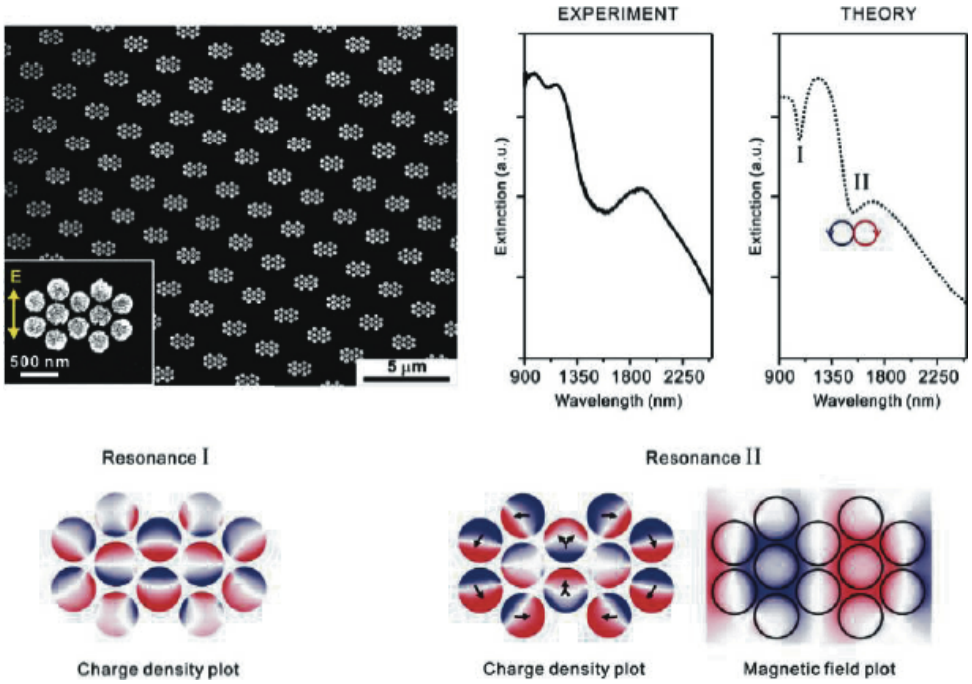

Figure 13 (online color at: www.lpr-journal.org) (a) Left: SEM image of a plasmonic naphthalene molecule. Right: experimental and simulated extinction spectra. The light polarization is along the direction of the two shared gold particles. Bottom: charge density and magnetic field plots at Resonances I and II. Resonance I corresponds to a double Fano resonance mode. Resonance II corresponds to a magnetic ring mode, in which antiphase magnetic plasmons are excited. (Adapted with permission from [239], © 2011, American Chemical Society.)

form all the substances in the universe and imagination to create a diverse range of new materials by combining atoms together into artificial molecules and solids.

3.7. Combination with other systems

Beyond the properties in pure plasmonic oligomer systems, their hybridization with other systems, such as quantum nanocrystal semiconductors [73, 243–246], is also a novel topic of research. Tanaka et al. [245] have reported recently that hybridizing semiconductor quantum dots with plasmonic systems leads to a multifold intensity increase and narrowing of their photoluminescence spectra. This luminescence enhancement can be precisely controlled by carefully designing the metallic nanostructures. A subsequent study by Manjavacas et al. [243] demonstrated the quantum internal evolution of hybrid systems beyond the perturbative regime. It is shown that the optical absorption spectrum of the plasmon-quantum-emitter system, which can be either a quantum emitter placed close to a metallic nanoparticle or in the gap of a nanoparticle dimer, respectively, can exhibit FRs resulting from the interaction between the quantum emitter and the plasmonic modes of the metal nanoparticles. This understanding is highly useful to describe plasmon–exciton interactions in the oligomers.

4. Ultrahigh-contrast Fano diode

Beyond the FR generation and identification methods and structures, a novel approach of Ding and coauthors [247] on the realization mechanism of FR generation is discussed. It was well explained [1, 2] that most FR shape realizations have been presented based on the classical definition of Fano that can be characterized by

$$T(\varepsilon) = \frac{f^2-1}{\varepsilon^2+1} + \frac{2f\varepsilon}{\varepsilon^2+1} + 1 = \frac{(\varepsilon+f)^2}{\varepsilon^2+1}, \qquad (3)$$

where $\varepsilon = \frac{2(\omega-\omega_0)}{\Gamma}$, ω, ω_0, and Γ are signal frequency, resonance center, and resonance linewidth. f is the Fano parameter that determines the degree of asymmetry. This Fano times formula (see Eq. (3)) can be understood as a superposition of the Lorentzian lineshape of the discrete level with a flat continuous background [1, 2]. Ding et al. [247] have recently interpreted the FR in a modified manner using the product of a Lorentzian line and a parabolic line. They designed a Fano spectrum with an arbitrary Fano factor, resonant center and linewidth using two cascaded but uncoupled cavities without interaction. By this method, FR can be realized by a cascaded inline-coupled cavity and a side-coupled cavity with proper separation. The new mechanism is independent of coupling between cavities, hence empowering tunable and reliable manipulation of directional signal transmission. This proves that the Fano formula, Eq. (3), can be decomposed into the product of a Lorentzian line and a parabolic line [247].

$$T(\varepsilon) = T_1 \cdot T_2 = \frac{1}{\varepsilon^2+1} \cdot (\varepsilon+f)^2. \qquad (4)$$

When two elements with response functions of T_1 and T_2 are designed separately and then cascade them together according to Eq. (4), a Fano-shaped line can be observed (see Fig. 14). In fact, the design of the presented effective Fano diodes [247] is based on this idea to decompose a Fano shape as a product of Lorentzian and parabolic line. It can highly benefit future research on FR generation and applications.

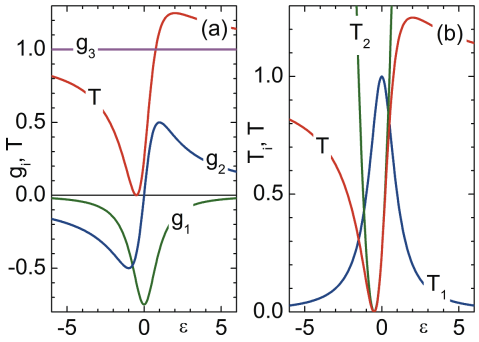

Figure 14 (online color at: www.lpr-journal.org) Schematic for the presentation of FR $T(\varepsilon)$ with $f = 1$ according to formula Eq. (3): $g_1 = \frac{f^2-1}{\varepsilon^2+1}$, $g_2 = \frac{2f\varepsilon}{\varepsilon^2+1}$, $g_3 = 1$ (a); and according to Eq. (4): $T_1 = \frac{1}{\varepsilon^2+1}$, $T_2 = (\varepsilon+f)^2$.

5. Applications

A few successful recent established applications of plasmonics FR are pointed out in the last part of this article. It should be mentioned that although science society has witnessed a significant growing number of research works published on FR generation in the past few years, the number of works presenting actual applications of FR is very small. But still among these few number of studies, some breakthroughs can be seen to pave the road towards physical applications of FR. For example, a Fano-resonant asymmetric metamaterial has been used as a platform for multispectral biosensing of nanometer-scale monolayers in the recognition of proteins and their surface orientation, as well as to detect chemical binding of target antibodies to recognize proteins [248]. In this outstanding approach, surface?enhanced infrared spectroscopy (SEIRS) and FRs are combined to achieve biosensing with structural resolution [249]. It was shown that by using infrared transparent substrates, it is possible to reveal conformational dynamics of biomolecules in their natural aqueous environment responsible for life-sustaining molecular-binding processes. This demonstrates the capabilities of metamaterial exhibiting FR for biosensing and fingerprinting ultrathin multiprotein layers. It was shown that the frequency of the subradiant resonance can be precisely determined and matched to the molecule's vibrational fingerprints. As compared to the earlier presented SEIRS sensor [250], this introduced FR-based platform shows a remarkable improvement of the sensor's performance by

one order of magnitude. But it should be noted that although this approach can identify the disease biomarkers in diagnostics therapeutics easier and safer, it still can be argued that in the presented method, the attached biochemical macromolecules should possess partial opacity. Therefore, in order to attach totally transparent objects to such a platform, an optical pulling force may be needed to attract these objects by using multipolar structures as pulling probes [251]. The results of Chen et al. [252] represented a clear understanding of optical forces, and the concept of the optical pulling force that can be used to further improve the breakthrough of Shvets and coworkers [248].

Furthermore, it has been shown that FR can be used in novel spectroscopic methods to determine nonlinear quantum-mechanical response functions beyond the optical diffraction limit. It can allow direct imaging of nanoscale coherence. Aeschlimann and coauthors achieved this by recording local nanospectra from a corrugated silver surface [253]. They observed subwavelength 2D lineshape variations by using four incident waves to detect the final state via photoemission electron microscopy at 50 nm spatial resolution. Plasmonic phase coherence of localized excitation can last for about 100 femtoseconds and exhibited coherent beats. With this application of 2D nanoscopy, different Fano-like resonances within one individual hot-spot emission can be resolved as well. It can be useful to define the shape of polarization pulses [254], which could allow the mapping of the tensor character of the nonlinear response by selecting the appropriate polarization directions of the excitation subpulses.

Meanwhile, Yu and coworkers [255] reported a novel approach in design of new photonic devices exhibiting FRs. They introduced a novel two-dimensional array of optical resonators with spatially varying phase response and subwavelength separation with abrupt phase changes over the scale of the wavelength [255]. The motivation is drawn from the fact that generally optical components rely on the gradual phase shifts accumulated during light propagation to shape light beams. They attained new degrees of freedom without contribution from propagation effects.

In another approach, Spinelli et al. [256] determined the coupling efficiency of FRs in the scattering, interparticle coupling and resonance shift in nanoparticle arrays placed on the top of a high refractive index substrate. It has been shown that a properly chosen array of Ag nanoparticles on a Si_3N_4 spacer layer can act as an excellent antireflection coating over a broad spectral range. It can lead to high impedance matching between light propagating in air and the substrate. Similarly Tittl et al. [257] reported a palladium-based plasmonic perfect absorber at visible wavelengths with a reflectance $< 0.5\%$ and zero transmittance at 650 nm by a design based on plasmonic palladium nanowires in combination with a dielectric spacer layer and a gold mirror. Furthermore, FR applications in enhanced magneto-optical effects [258, 259], ultrasharp nonlinear photothermal resonances [260], nonlinear spectroscopy [261], phase-sensitive measurements [262] and photoabsorption of nanoclusters in helium droplets [263] are some of other high-impact achievements in recent years.

6. Conclusions

In summary, we have reviewed recent progress in the field of FR in plasmonic structures. We have shown that the developed nanofabrication techniques available for plasmonics structures as well as recent advancements in nano-optical characterization, and improvements in full-field computational electromagnetics have provided rich opportunities to study the near-field and far-field optical properties of newly proposed nanostructures that exhibit FRs. Meanwhile, more attention has been given to plasmonic oligomers as a densely packed arrangement of metallic nanoparticles in which the sharp FR excitation is based on the coupling of the antiparallel dipole modes. Oligomers are able to exhibit polarization-independent far-field optical properties including FR, while the near-field characteristics are highly polarization dependent. The effects of the number of components as well as their geometry, size, material and interparticle gap on the optical properties of oligomers have been reviewed in detail. A general recipe to tailor the overall spectral profile of oligomers is also described. Finally, a brief overview of the recent successful applications of plasmonic FR has been provided.

Acknowledgements. The authors acknowledge funding provided by SERC Agency of Science, Technology and Research (A*STAR) Superlens Program (Project No. 092 154 0099) and A*STAR TSRP Program, grant No. 102 152 0018. In addition, the authors thank Prof. Harald Giessen, Prof. Peter. Nordlander, Prof. Stefan A. Maier, Prof. Andrey Miroshnichenko, Prof. Thomas Yun Fook Liew, Dr. Vincenzo Giannini and Dr. Mario Hentschel for useful discussion and comments as well as Dr. Dang Yuan Lei for FTIR measurements and Dr. Mojtaba Ranjbar for AFM images. Mohsen Rahmani would like to express his gratitude for the support from the A*STAR – SINGA program.

Received: 23 April 2012, **Revised:** 29 May 2012,
Accepted: 18 June 2012

Published online: 24 July 2012

Key words: Fano resonance, surface plasmons, subwavelength nanostructures, plasmonic oligomers, near-field energy distribution.

Mohsen Rahmani received the M. Sc. in Laser Technology at Kiev Polytechinic Institute (KPI), Ukraine in 2007. He was at KPI University from 2007 to 2009, working with high-power laser machining. In 2009 he was awarded by the Agency of Science Technology And Research (A*STAR) to pursue his PhD study in the Department of Electrical and Computer Engineering of the National University of Singapore. His research interests are in plasmonic and terahertz metamaterials.

Boris Luk'yanchuk graduated from the Moscow State University in 1967, PhD (1979) from the P.N. Lebedev Physical Institute, Russian Academy of Sciences and Doctor of Sciences (1991) from the General Physics Institute, Russian Academy of Sciences. He got State Professor degree in 1992 and was head of the Laboratory at the General Physics Institute, Russian Academy of Sciences till 2000. Since 1999 he has been working at the Data Storage Institute A*STAR, Singapore. He is an Honorary Professor at Johannes Kepler University, Linz, Austria and a Fellow of the Optical Society of America (OSA).

Minghui Hong received his PhD degree in 2000 in the National University of Singapore (NUS). He became Assistant Professor in 2003 and Associate Professor in 2007 in the Department of Electrical and Computer Engineering of NUS. His research interests are laser microprocessing and nanofabrication, terahertz systems technology and plasmonics. He is a Fellow of the Optical Society of America (OSA) and International Society for Optics and Photonics (SPIE).

References

[1] B. Luk'yanchuk, N. I. Zheludev, S. A. Maier, N. J. Halas, P. Nordlander, H. Giessen, and C. T. Chong, Nature Mater. **9**, 707–715 (2010).
[2] A. E. Miroshnichenko, S. Flach, and Y. S. Kivshar, Rev. Mod. Phys. **82**, 2257–2298 (2010).
[3] U. Fano, Nuovo Cimento **12**, 8 (1935).
[4] U. Fano, Phys. Rev. **124**, 1866–1878 (1961).
[5] M. I. Rabinovitch, and D. I. Trubetskov, Oscillations and Waves in Linear and Nonlinear Systems (Kluwer Academic Publishers, Dordrecht, 1989).
[6] R. Franco, M. S. Figueira, and E. V. Anda, Phys. Rev. B **67**, 155301 (2003).
[7] A. C. Johnson, C. M. Marcus, M. P. Hanson, and A. C. Gossard, Phys. Rev. B **71**, 115333 (2005).
[8] K. Kobayashi, H. Aikawa, A. Sano, S. Katsumoto, and Y. Iye, Phys. Rev. B **70**, 035319 (2004).
[9] Y. Alhassid, Y. V. Fyodorov, T. Gorin, W. Ihra, and B. Mehlig, Phys. Rev. A **73**, 042711 (2006).
[10] T. H. Hoffmann, M. Allan, K. Franz, M. W. Ruf, H. Hotop, G. Sauter, and W. Meyer, J. Phys. B-At. Mol. Opt. **42**, 211001 (2009).
[11] S. Mukhopadhyay, R. Biswas, and C. Sinha, J. Appl. Phys. **110**, 014306 (2011).
[12] S. Mukhopadhyay, R. Biswas, and C. Sinha, Phys. Lett. A **375**, 2921–2927 (2011).
[13] H. G. Luo, T. Xiang, X. Q. Wang, Z. B. Su, and L. Yu, Phys. Rev. Lett. **92**, 256602 (2004).
[14] M. V. Rybin, A. B. Khanikaev, M. Inoue, A. K. Samusev, M. J. Steel, G. Yushin, and M. F. Limonov, Photon. Nanostruct. **8**, 86–93 (2010).
[15] M. V. Rybin, A. B. Khanikaev, M. Inoue, K. B. Samusev, M. J. Steel, G. Yushin, and M. F. Limonov, Phys. Rev. Lett. **103**, 023901 (2009).
[16] I. A. I. Al-Naib, C. Jansen, N. Born, and M. Koch, Appl. Phys. Lett. **98**, 091107 (2011).
[17] Z. Chen, M. Rahmani, G. Yandong, C. T. Chong, and M. H. Hong, Adv. Mater. **24**, OP143–OP147 (2012).
[18] Z. C. Chen, M. H. Hong, C. S. Lim, N. R. Han, L. P. Shi, and T. C. Chong, Appl. Phys. Lett. **96**, 3424793 (2010).
[19] C. Jansen, I. A. I. Al-Naib, N. Born, and M. Koch, Appl. Phys. Lett. **98**, 051109 (2011).
[20] Z. Li, Y. Ma, R. Huang, R. Singh, J. Gu, Z. Tian, J. Han, and W. Zhang, Opt. Express **19**, 8912–8919 (2011).
[21] Y. Ma, Z. Li, Y. Yang, R. Huang, R. Singh, S. Zhang, J. Gu, Z. Tian, J. Han, and W. Zhang, Opt. Mater. Express **1**, 391–399 (2011).
[22] A. E. Nikolaenko, N. Papasimakis, A. Chipouline, F. DeAngelis, E. DiFabrizio, and N. I. Zheludev, Opt. Express **20**, 6068–6079 (2012).
[23] B. Pradarutti, G. Torosyan, M. Theuer, and R. Beigang, Appl. Phys. Lett. **97**, 244103 (2010).
[24] R. Singh, I. A. I. Al-Naib, M. Koch, and W. Zhang, Opt. Express **19**, 6312–6319 (2011).
[25] R. Singh, I. A. I. Al-Naib, Y. Yang, D. Roy Chowdhury, W. Cao, C. Rockstuhl, T. Ozaki, R. Morandotti, and W. Zhang, Appl. Phys. Lett. **99**, 201107 (2011).
[26] A. P. Sukhorukov, D. O. Ignatyeva, and A. N. Kalish, J. Infrared Millim. **32**, 1223–1235 (2011).
[27] A. Tuniz, R. Lwin, A. Argyros, S. C. Fleming, E. M. Pogson, E. Constable, R. A. Lewis, and B. T. Kuhlmey, Opt. Express **19**, 16480–16490 (2011).
[28] X. Xiao, J. Wu, F. Miyamaru, M. Zhang, S. Li, M. W. Takeda, W. Wen, and P. Sheng, Appl. Phys. Lett. **98**, 011911 (2011).
[29] M. Agio, Nanoscale **4**, 692–706 (2012).
[30] P. Biagioni, J. S. Huang, and B. Hecht, Rep. Prog. Phys. **75,** 40 (2012).
[31] A. I. Fernández-Domínguez, and S. A. Maier, IEEE Photon. J. **3**, 284–287 (2011).
[32] D. Y. Lei, K. Appavoo, Y. Sonnefraud, R. F. Haglund Jr, and S. A. Maier, Opt. Lett. **35**, 3988–3990 (2010).
[33] D. Y. Lei, A. Aubry, S. A. Maier, and J. B. Pendry, New J. Phys. **12**, 093030 (2010).
[34] D. Y. Lei, A. I. Fernández-Domínguez, Y. Sonnefraud, K. Appavoo, R. F. Haglund Jr, J. B. Pendry, and S. Maier, ACS Nano **6**, 1380–1386 (2012).
[35] S. Maier, Plasmonics: Fundamentals and Applications (Springer, Berlin, 2007).
[36] S. A. Maier, in: Proceedings of the Photonics Society Summer Topical Meeting Series, 2010 IEEE, London, UK, 2010, pp. 66–67.
[37] F. Papoff, and B. Hourahine, arXiv:1102.4958v1 4 (2011).
[38] E. Petryayeva, and U. J. Krull, Analytica. Chimica. Acta **706**, 8–24 (2011).
[39] M. I. Stockman, Opt. Express **19**, 22029–22106 (2011).
[40] T. Utikal, T. Zentgraf, T. Paul, C. Rockstuhl, F. Lederer, M. Lippitz, and H. Giessen, Phys. Rev. Lett. **106**, 133901 (2011).
[41] W. Zhang, B. Gallinet, and O. J. F. Martin, Phys. Rev. B **81**, 235427 (2010).
[42] V. Giannini, A. I. Fernández-Domínguez, S. C. Heck, and S. A. Maier, Chem. Rev. **111**, 3888–3912 (2011).

[43] N. J. Halas, S. Lal, W. S. Chang, S. Link, and P. Nordlander, Chem. Rev. **111**, 3913–3961 (2011).
[44] M. R. Jones, K. D. Osberg, R. J. MacFarlane, M. R. Langille, and C. A. Mirkin, Chem. Rev. **111**, 3736–3827 (2011).
[45] A. E. Miroshnichenko, S. Flach, A. V. Gorbach, B. S. Luk'yanchuk, Y. S. Kivshar, and M. I. Tribelsky, Opt. Photon. News **19**, 48 (2008).
[46] P. Alonso-Gonzalez, M. Schnell, P. Sarriugarte, H. Sobhani, C. Wu, N. Arju, A. Khanikaev, F. Golmar, P. Albella, L. Arzubiaga, F. Casanova, L. E. Hueso, P. Nordlander, G. Shvets, and R. Hillenbrand, Nano Lett. **11**, 3922–3926 (2011).
[47] K. Bao, N. A. Mirin, and P. Nordlander, Appl. Phys. A **100**, 333–339 (2010).
[48] D. Dregely, M. Hentschel, and H. Giessen, ACS Nano **5**, 8202–8211 (2011).
[49] J. A. Fan, K. Bao, C. Wu, J. Bao, R. Bardhan, N. J. Halas, V. N. Manoharan, G. Shvets, P. Nordlander, and F. Capasso, Nano Lett. **10**, 4680–4685 (2010).
[50] J. A. Fan, Y. He, K. Bao, C. Wu, J. Bao, N. B. Schade, V. N. Manoharan, G. Shvets, P. Nordlander, D. R. Liu, and F. Capasso, Nano Lett. **11**, 4859–4864 (2011).
[51] J. A. Fan, C. Wu, K. Bao, J. Bao, R. Bardhan, N. J. Halas, V. N. Manoharan, P. Nordlander, G. Shvets, and F. Capasso, Science **328**, 1135–1138 (2010).
[52] M. Hentschel, D. Dregely, R. Vogelgesang, H. Giessen, and N. Liu, ACS Nano **5**, 2042–2050 (2011).
[53] M. Hentschel, N. Liu, D. Dregely, and H. Giessen, in: Proceedings of the Quantum Electronics and Laser Science Conference (QELS), Baltimore, USA, 2011, paper QFA5.
[54] M. Hentschel, M. Saliba, R. Vogelgesang, H. Giessen, A. P. Alivisatos, and N. Liu, Nano Lett. **10**, 2721–2726 (2010).
[55] J. B. Lassiter, H. Sobhani, J. A. Fan, J. Kundu, F. Capasso, P. Nordlander, and N. J. Halas, Nano Lett. **10**, 3184–3189 (2010).
[56] T. C. M. Frimmer, and A. F. Koenderink, arXiv:1109.5407v1 (2011).
[57] M. Rahmani, B. Lukiyanchuk, B. Ng, A. K. G. Tavakkoli, Y. F. Liew, and M. H. Hong, Opt. Express **19**, 4949–4956 (2011).
[58] M. Rahmani, B. Lukiyanchuk, T. T. V. Nguyen, T. Tahmasebi, Y. Lin, T. Y. F. Liew, and M. H. Hong, Opt. Mater. Express **1**, 1409–1415 (2011).
[59] M. Rahmani, B. Lukiyanchuk, T. Tahmasebi, Y. Lin, T. Y. F. Liew, and M. H. Hong, Appl. Phys. A **107**, 23–30 (2011).
[60] M. Rahmani, T. Tahmasebi, Y. Lin, B. Lukiyanchuk, T. Y. F. Liew, and M. H. Hong, Nanotechnology **22**, 245204 (2011).
[61] S. N. Sheikholeslami, A. García-Etxarri, and J. A. Dionne, Nano Lett. **11**, 3927–3934 (2011).
[62] B. Yan, S. V. Boriskina, and B. M. Reinhard, J. Phys. Chem. C **115**, 4578–4583 (2011).
[63] S. I. Bozhevolnyi, A. B. Evlyukhin, A. Pors, M. G. Nielsen, M. Willatzen, and O. Albrektsen, New J. Phys. **13**, 023034 (2011).
[64] A. Farhang, and O. J. F. Martin, Opt. Express **19**, 11387–11396 (2011).
[65] B. Gallinet and O. J. F. Martin, in: Proceedings of Progress in Electromagnetics Research Symposium (PIERS), Kuala Lumpur, Malaysia, 2012, pp. 775–776
[66] B. Gallinet, and O. J. F. Martin, Opt. Express **19**, 22167–22175 (2011).
[67] B. Gallinet, and O. J. F. Martin, Phys. Rev. B **83**, 235427 (2011).
[68] V. Giannini, Y. Francescato, H. Amrania, C. C. Phillips, and S. A. Maier, Nano Lett. **11**, 2835–2840 (2011).
[69] D. V. Novitsky, Opt. Lett. **36**, 2002–2004 (2011).
[70] F. Papoff, and B. Hourahine, Opt. Express **19**, 21432–21444 (2011).
[71] A. Pors, M. Willatzen, O. Albrektsen, and S. I. Bozhevolnyi, Phys. Rev. B **83**, 245409 (2011).
[72] D. M. Riffe, Phys. Rev. B **84**, 064308 (2011).
[73] W. Zhang, and A. O. Govorov, Phys. Rev. B **84**, 081405(R) (2011).
[74] J. Zuloaga, and P. Nordlander, Nano Lett. **11**, 1280–1283 (2011).
[75] A. Artar, A. A. Yanik, and H. Altug, Nano Lett. **11**, 1685–1689 (2011).
[76] K. Aydin, I. M. Pryce, and H. A. Atwater, Opt. Express **18**, 13407–13417 (2010).
[77] A. Bitzer, J. Wallauer, H. Helm, H. Merbold, T. Feurer, and M. Walther, Opt. Express **17**, 22108–22113 (2009).
[78] S. Campione, A. Vallecchi, M. Albani, F. Mesa, and F. Capolino, in: Proceedings of the SPIE Villa Conference on Metamaterials, Las Vegas, USA, 2011, paper 775738.
[79] R. L. Chern, and W. T. Hong, J. Opt. **12**, 065101 (2010).
[80] Z. G. Dong, H. Liu, M. X. Xu, T. Li, S. M. Wang, J. X. Cao, S. N. Zhu, and X. Zhang, Opt. Express **18**, 22412–22417 (2010).
[81] X. Fan, Z. Shen, and B. Luk'yanchuk, Opt. Express **18**, 24868–24880 (2010).
[82] M. Geiselmann, T. Utikal, M. Lippitz, and H. Giessen, Phys. Rev. B **81**, 235101 (2010).
[83] D. E. Gómez, K. C. Vernon, and T. J. Davis, Phys. Rev. B **81**, 075414 (2010).
[84] T. G. Habteyes, S. Dhuey, S. Cabrini, P. J. Schuck, and S. R. Leone, Nano Lett. **11**, 1819–1825 (2011).
[85] F. Hao, P. Nordlander, Y. Sonnefraud, P. Van Dorpe, and S. A. Maier, ACS Nano **3**, 643–652 (2009).
[86] F. Hao, Y. Sonnefraud, P. Van Dorpe, S. A. Maier, N. J. Halas, and P. Nordlander, Nano Lett. **8**, 3983–3988 (2008).
[87] S. Iyer, S. Popov, and A. T. Friberg, Appl. Opt. **50**, 3958–3961 (2011).
[88] J. Shi, Zh. Zhu, Ch. Guan, Y. Li, and Z. Wang, in: Proceedings of Advances in Optoelectronics and Micro/Nano-Optics (AOM), Harbin, China, 2010, pp. 1–3.
[89] B. Kang, E. Choi, H. H. Lee, E. S. Kim, J. H. Woo, J. Kim, T. Y. Hong, J. H. Kim, and J. W. Wu, Opt. Express **18**, 11552–11561 (2010).
[90] M. Kang, H. X. Cui, Y. Li, B. Gu, J. Chen, and H. T. Wang, J. Appl. Phys. **109**, 014901 (2011).
[91] S. A. Maier, Nature Mater. **8**, 699–700 (2009).
[92] F. Neubrech, A. Garcia-Etxarri, D. Weber, J. Bochterle, H. Shen, M. Lamy De La Chapelle, G. W. Bryant, J. Aizpurua, and A. Pucci, Appl. Phys. Lett. **96**, 213111 (2010).
[93] R. Ortu, ño, C. García-Meca, F. J. Rodríguez-Fortuño, J. Mart, í, and A. Martínez, Opt. Express **18**, 7893–7898 (2010).
[94] R. Ortu, ño, C. García-Meca, F. J. Rodríguez-Fortuño, and A. Martínez, Opt. Lett. **35**, 4205–4207 (2010).
[95] E. Plum, K. Tanaka, W. T. Chen, V. A. Fedotov, D. P. Tsai, and N. I. Zheludev, J. Opt. **13**, 055102 (2011).

[96] J. Shi, C. Guan, and Z. Wang, Phot. Nano. Fund. Appl. **9**, 255–260 (2011).
[97] P. J. Schuck, Z. Zhang, A. Weber-Bargioni, Sh. Wu, S. Dhuey, and S. Cabrini, in: Proceedings of the Quantum Electronics and Laser Science Conference (QELS), San Jose, USA, 2010, paper QFAS.
[98] X. R. Su, Z. S. Zhang, L. H. Zhang, Q. Q. Li, C. C. Chen, Z. J. Yang, and Q. Q. Wang, Appl. Phys. Lett. **96**, 043113 (2010).
[99] A. Vallecchi, S. Campione, and F. Capolino, J. Nanophoton. **4**, 041577 (2010).
[100] N. Verellen, Y. Sonnefraud, H. Sobhani, F. Hao, V. V. Moshehalkov, P. Van Dorpe, P. Nordlander, and S. A. Maier, Nano Lett. **9**, 1663–1667 (2009).
[101] D. Weber, P. Albella, P. Alonso-Gonz, ález, F. Neubrech, H. Gui, T. Nagao, R. Hillenbrand, J. Aizpurua, and A. Pucci, Opt. Express **19**, 15047–15061 (2011).
[102] S. C. Yang, H. Kobori, C. L. He, M. H. Lin, C. Hung-Ying, C. Li, M. Kanehara, T. Teranishi, and S. Gwo, Nano Lett. **10**, 632–637 (2010).
[103] A. Yar, A. Donarini, S. Koller, and M. Grifoni, Phys. Rev. B **84**, 115432 (2011).
[104] J. Ye, P. V. Dorpe, W. V. Roy, K. Lodewijks, I. D. Vlaminck, G. Borghs, and G. Maes, J. Phys. Chem. C **113**, 3110–3115 (2009).
[105] J. Ye, L. Lagae, G. Maes, G. Borghs, and P. Van Dorpe, Opt. Express **17**, 23765–23771 (2009).
[106] J. Ye, N. Verellen, W. Van Roy, L. Lagae, G. Maes, G. Borghs, and P. Van Dorpe, ACS Nano **4**, 1457–1464 (2010).
[107] Z. Zhang, A. Weber-Bargioni, S. W. Wu, S. Dhuey, S. Cabrini, and P. J. Schuck, Nano Lett. **9**, 4505–4509 (2009).
[108] J. I. Ziegler, and R. F. Haglund Jr, Nano Lett. **10**, 3013–3018 (2010).
[109] J. I. Ziegler, J. Nag, and R. F. Haglund, Jr, in: Proceedings of Plasmonics: Metallic Nanostructures and Their Optical Properties VII, San Diego, USA, 2009, paper 7394.
[110] Z. Fang, J. Cai, Z. Yan, N. K. Grady, and X. Zhu, arXiv:1105.1568v1 (2011).
[111] Z. Fang, J. Cai, Z. Yan, P. Nordlander, N. J. Halas, and X. Zhu, Nano Lett. **11**, 4475–4479 (2011).
[112] L. J. Sherry, S. H. Chang, G. C. Schatz, R. P. Van Duyne, B. J. Wiley, and Y. Xia, Nano Lett. **5**, 2034–2038 (2005).
[113] S. Zhang, K. Bao, N. J. Halas, H. Xu, and P. Nordlander, Nano Lett. **11**, 1657–1663 (2011).
[114] G. Toscano, S. Raza, A. P. Jauho, N. A. Mortensen, and M. Wubs, Opt. Express **20**, 4176–4188 (2012).
[115] W. Ahn, S. V. Boriskina, Y. Hong, and B. M. Reinhard, ACS Nano **6**, 951–960 (2012).
[116] V. I. Belotelov, A. N. Kalish, A. K. Zvezdin, A. V. Gopal, and A. S. Vengurlekar, J. Opt. Soc. Am. B **29**, 294–299 (2012).
[117] Y. H. Fu, J. B. Zhang, Y. F. Yu, and B. Luk'yanchuk, ACS Nano **6**, 2130–2137 (2012).
[118] S. V. Boriskina, and B. M. Reinhard, Opt. Express **19**, 22305–22315 (2011).
[119] H. Chen, L. Shao, T. Ming, K. C. Woo, Y. C. Man, J. Wang, and H. Q. Lin, ACS Nano **5**, 6754–6763 (2011).
[120] J. Chen, P. Wang, C. Chen, Y. Lu, H. Ming, and Q. Zhan, Opt. Express **19**, 5970–5978 (2011).
[121] W. Chen, G. Y. Chen, and Y. N. Chen, Opt. Lett. **36**, 3602–3604 (2011).
[122] W. J. Chen, J. C. W. Lee, J. W. Dong, C. W. Qiu, and H. Z. Wang, Appl. Phys. Lett. **98**, 081116 (2011).
[123] W. T. Chen, C. J. Chen, P. C. Wu, S. Sun, L. Zhou, G. Y. Guo, C. T. Hsiao, K. Y. Yang, N. I. Zheludev, and D. P. Tsai, Opt. Express **19**, 12837–12842 (2011).
[124] Y. Chu, D. Wang, W. Zhu, and K. B. Crozier, Opt. Express **19**, 14919–14928 (2011).
[125] M. R. Disfani, M. S. Abrishamian, and P. Berini, Opt. Express **20**, 6472–6477 (2012).
[126] B. Fazio, C. D'Andrea, F. Bonaccorso, A. Irrera, G. Calogero, C. Vasi, P. G. Gucciardi, M. Allegrini, A. Toma, D. Chiappe, C. Martella, and F. Buatier De Mongeot, ACS Nano **5**, 5945–5956 (2011).
[127] Y. H. Fu, A. Q. Liu, W. M. Zhu, X. M. Zhang, D. P. Tsai, J. B. Zhang, T. Mei, J. F. Tao, H. C. Guo, X. H. Zhang, J. H. Teng, N. I. Zheludev, G. Q. Lo, and D. L. Kwong, Adv. Funct. Mater. **21**, 3589–3594 (2011).
[128] W. Ahn, S. V. Boriskina, Y. Hong, and B. M. Reinhard, Nano Lett. **12**, 219–227 (2012).
[129] Y. He, H. Zhou, Y. Jin, and S. He, Appl. Phys. Lett. **99**, 043113 (2011).
[130] L. Dal Negro, and S. V. Boriskina, Laser Photon. Rev. **6**, 178–218 (2011).
[131] Y. W. Huang, Y. T. Chen, P. C. Wu, V. Fedotov, V. Savinov, Y. Z. Ho, Y. F. Chau, N. I. Zheludev, and D. P. Tsai, Opt. Express **20**, 1760–1761 (2012).
[132] H. Husu, J. Mäkitalo, R. Siikanen, G. Genty, H. Pietarinen, J. Lehtolahti, J. Laukkanen, M. Kuittinen, and M. Kauranen, Opt. Lett. **36**, 2375–2377 (2011).
[133] L. Langguth, and H. Giessen, Opt. Express **19**, 22156–22166 (2011).
[134] C. T. Li, H. F. Chen, L. W. Un, H. C. Lee, and T. J. Yen, Opt. Express **20**, 3250–3260 (2012).
[135] C. S. Lim, M. H. Hong, Z. C. Chen, N. R. Han, B. Luk'Yanchuk, and T. C. Chong, Opt. Express **18**, 12421–12429 (2010).
[136] Y. Liu, H. Jiang, C. Xue, W. Tan, H. Chen, and Y. Shi, Prog. Electromagnet. Res. Lett. **26**, 49–57 (2011).
[137] F. López-Tejeira, R. Paniagua-Domínguez, R. Rodríguez-Oliveros, and J. A. Sánchez-Gil, New J. Phys. **14**, 23035–23050 (2012).
[138] H. Lu, X. Liu, D. Mao, Y. Gong, and G. Wang, Opt. Lett. **36**, 3233–3235 (2011).
[139] Y. Lu, X. Jin, S. Lee, J. Y. Rhee, W. H. Jang, and Y. P. Lee, Adv. Nature Sci. Nanosci. Nanotechnol. **1**, 045004 (2010).
[140] C. T. Chong, M. H. Hong, and L. P. Shi, Laser Photon. Rev. **4**, 123–143 (2009).
[141] S. H. Mousavi, A. B. Khanikaev, and G. Shvets, arXiv:1201.3146v1 (2012).
[142] D. Nardi, M. Travagliati, M. E. Siemens, Q. Li, M. M. Murnane, H. C. Kapteyn, G. Ferrini, F. Parmigiani, and F. Banfi, Nano Lett. **11**, 4126–4133 (2011).
[143] M. G. Nielsen, A. Pors, O. Albrektsen, M. Willatzen, and S. I. Bozhevolnyi, J. Opt. **13**, 055106 (2011).
[144] L. Niu, J. B. Zhang, Y. H. Fu, S. Kulkarni, and B. Lukiyanchuk, Opt. Express **19**, 22974–22981 (2011).
[145] P. Offermans, M. C. Schaafsma, S. R. K. Rodriguez, Y. Zhang, M. Crego-Calama, S. H. Brongersma, and J. Gómez Rivas, ACS Nano **5**, 5151–5157 (2011).
[146] N. Papasimakis, V. A. Fedotov, Y. H. Fu, D. P. Tsai, and N. I. Zheludev, Phys. Rev. B **80**, 014509 (2009).

[147] N. Papasimakis, Y. H. Fu, V. A. Fedotov, S. L. Prosvirnin, D. P. Tsai, and N. I. Zheludev, Appl. Phys. Lett. **94**, 211902 (2009).
[148] S. Peng, C. Qiu, Z. He, Y. Ye, S. Xu, K. Tang, M. Ke, and Z. Liu, J. Appl. Phys. **110**, 014509 (2011).
[149] J. M. Reed, H. Wang, W. Hu, and S. Zou, Opt. Lett. **36**, 4386–4388 (2011).
[150] A. Ridolfo, R. Saija, S. Savasta, P. H. Jones, M. A. Iatì, and O. M. Maragò, ACS Nano **5**, 7354–7361 (2011).
[151] A. Santillán, and S. I. Bozhevolnyi, Phys. Rev. B **84**, 064304 (2011).
[152] H. Wang, C. Sheppard, K. Ravi, S. T. Ho, and G. Vinne, Laser Photon. Rev. **6**, 354–392 (2012).
[153] M. Abb, P. Albella, J. Aizpurua, and O. L. Muskens, ACS Nano **11**, 2457–2463 (2011).
[154] Y. Sonnefraud, N. Verellen, H. Sobhani, G. A. E. Vandenbosch, V. V. Moshchalkov, P. Van Dorpe, P. Nordlander, and S. A. Maier, ACS Nano **4**, 1664–1670 (2010).
[155] P. Spinelli, V. E. Ferry, J. V. D. Groep, M. V. Lare, M. A. Verschuuren, R. E. I. Schropp, H. A. Atwater, and A. Polman, J. Opt. **14**, 11 (2012).
[156] Y. Sun, H. Jiang, Y. Yang, Y. Zhang, H. Chen, and S. Zhu, Phys. Rev. B **83**, 195140 (2011).
[157] B. Tang, L. Dai, and C. Jiang, Opt. Express **19**, 628–637 (2011).
[158] S. Toroghi, and P. G. Kik, Phys. Rev. B **85**, 045432 (2012).
[159] T. Utikal, T. Zentgraf, S. G. Tikhodeev, M. Lippitz, and H. Giessen, Phys. Rev. B **84**, 133901 (2011).
[160] N. Verellen, P. Van Dorpe, D. Vercruysse, G. A. E. Vandenbosch, and V. V. Moshchalkov, Opt. Express **19**, 11034–11051 (2011).
[161] C. Wu, A. B. Khanikaev, and G. Shvets, Phys. Rev. Lett. **106**, 107403 (2011).
[162] Y. Xu, and A. E. Miroshnichenko, Europhys. Lett. **97**, 44007 (2012).
[163] E. Ye, K. Y. Win, H. R. Tan, M. Lin, C. P. Teng, A. Mlayah, and M. Y. Han, J. Am. Chem. Soc. **133**, 8506–8509 (2011).
[164] X. G. Yin, C. P. Huang, Q. J. Wang, W. X. Huang, L. Zhou, C. Zhang, and Y. Y. Zhu, Opt. Express **19**, 10485–10493 (2011).
[165] L. Zhu, F. Y. Meng, J. H. Fu, Q. Wu, and J. Hua, Opt. Express **20**, 4494–4502 (2012).
[166] N. Verellen, P. Van Dorpe, C. Huang, K. Lodewijks, G. A. E. Vandenbosch, L. Lagae, and V. V. Moshchalkov, Nano Lett. **11**, 391–397 (2011).
[167] A. Artar, A. A. Yanik, and H. Altug, Nano Lett. **11**, 1685–1689 (2011).
[168] G. X. Li, Z. L. Wang, S. M. Chen, and K. W. Cheah, Opt. Express **19**, 6348–6353 (2011).
[169] L. Lin, and A. Roberts, Opt. Express **19**, 2626–2633 (2011).
[170] H. Liu, N. Wang, Y. Liu, Y. Zhao, and X. Wu, Opt. Lett. **36**, 385–387 (2011).
[171] M. Liu, Y. Song, Y. Zhang, X. Wang, and C. Jin, Plasmonics DOI: 10.1007/s11468-011-9321-5 (2012).
[172] P. Lovera, D. Jones, and A. O'Riordan, J. Phys. Con. Ser. **307**, 012006 (2011).
[173] J. Zhang, J. Y. Ou, N. Papasimakis, Y. Chen, K. F. MacDonald, and N. Zheludev, Opt. Express **19**, 623279–23285 (2011).
[174] S. Feng, X. Zhang, and P. J. Klar, Appl. Phys. Lett. **99**, 053119 (2011).
[175] Y. Huang, C. Min, and G. Veronis, in: Proceedings of Integrated Optics: Devices, Materials, and Technologies XV, San Francisco, USA, 2011, paper 79410X.
[176] M. Pohl, V. I. Belotelov, I. A. Akimov, S. Kasture, A. S. Vengurlekar, A. V. Gopal, A. K. Zvezdin, D. R. Yakovlev, and M. Bayer, Phys. Rev. B **85**, 081401 (2012).
[177] P. Pottier, L. Shi, and Y. A. Peter, J. Opt. Soc. Am. B **29**, 109–117 (2012)
[178] E. Sakat, G. Vincent, P. Ghenuche, N. Bardou, S. Collin, F. Pardo, J. L. Pelouard, and R. Haïdar, Opt. Lett. **36**, 3054–3056 (2011).
[179] P. Schau, K. Frenner, L. Fu, H. Schweizer, H. Giessen, and W. Osten, Opt. Express **19**, 3627–3636 (2011).
[180] M. R. Shcherbakov, P. P. Vabishchevich, V. V. Komarova, T. V. Dolgova, and A. A. Fedyanin, arXiv:1105.4730 (2011).
[181] A. Christ, S. G. Tikhodeev, N. A. Gippius, J. Kuhl, and H. Giessen, Phys. Rev. Lett. **91**, 183901 (2003).
[182] N. T. Fofang, N. K. Grady, Z. Fan, A. O. Govorov, and N. J. Halas, Nano Lett. **11**, 1556–1560 (2011).
[183] A. I. Kuznetsov, A. B. Evlyukhin, M. R. Go, alves, C. Reinhardt, A. Koroleva, M. L. Arnedillo, R. Kiyan, O. Marti, and B. N. Chichkov, ACS Nano **5**, 4843–4849 (2011).
[184] S. Mühlig, A. Cunningham, S. Scheeler, C. Pacholski, T. Bürgi, C. Rockstuhl, and F. Lederer, ACS Nano **5**, 6586–6592 (2011).
[185] S. Mühlig, C. Rockstuhl, V. Yannopapas, T. Bürgi, N. Shalkevich, and F. Lederer, Opt. Express **19**, 9607–9616 (2011).
[186] S. Mukherjee, H. Sobhani, J. B. Lassiter, R. Bardhan, P. Nordlander, and N. J. Halas, Nano Lett. **10**, 2694–2701 (2010).
[187] M. Wang, M. Cao, X. Chen, and N. Gu, J. Phys. Chem. C **115**, 20920–20925 (2011).
[188] D. Wu, S. Jiang, and X. Liu, J. Phys. Chem. C **115**, 23797–23801 (2011).
[189] J. F. Ho, B. Luk'yanchuk, and J. B. Zhang, Appl. Phys. A **107**, 133–137 (2012).
[190] H. Wang, Y. Wu, B. Lassiter, C. L. Nehl, J. H. Hafner, P. Nordlander, and M. J. Halas, Proc. Natl. Acad. Sci. USA **103**, 10856–10860 (2006).
[191] L. V. Brown, H. Sobhani, J. B. Lassiter, P. Nordlander, and N. J. Halas, ACS Nano **4**, 819–832 (2010).
[192] Y. T. Chen, R. L. Chern, and H. Y. Lin, Appl. Opt. **49**, 2819–2826 (2010).
[193] Z. G. Dong, H. Liu, M. X. Xu, T. Li, S. M. Wang, S. N. Zhu, and X. Zhang, Opt. Express **18**, 18229–18234 (2010).
[194] G. F. Walsh, C. Forestiere, and L. Dal Negro, Opt. Express **19**, 21081–21090 (2011).
[195] K. C. Woo, L. Shao, H. Chen, Y. Liang, J. Wang, and H. Q. Lin, ACS Nano **5**, 5976–5986 (2011).
[196] Z. J. Yang, Z. S. Zhang, Z. H. Hao, and Q. Q. Wang, Appl. Phys. Lett. **99**, 081107 (2011).
[197] Z. J. Yang, Z. S. Zhang, L. H. Zhang, Q. Q. Li, Z. H. Hao, and Q. Q. Wang, Opt. Lett. **36**, 1542–1544 (2011).
[198] A. B. Evlyukhin, S. I. Bozhevolnyi, A. Pors, M. G. Nielsen, I. P. Radko, M. Willatzen, and O. Albrektsen, Nano Lett. **10**, 4571–4577 (2010).
[199] T. Shegai, S. Chen, V. D. Miljkovi, ć, G. Zengin, P. Johansson, and M. Käll, Nature Commun. **2**, 481 (2011).
[200] S. Aksu, M. Huang, A. Artar, A. A. Yanik, S. Selvarasah, M. R. Dokmeci, and H. Altug, Adv. Mater. **23**, 4422–4430 (2011).

[201] H. Duan, H. Hu, K. Kumar, Z. Shen, and J. K. W. Yang, ACS Nano **5**, 7593–7600 (2011).
[202] A. K. G. Tavakkoli, S. N. Piramanayagam, M. Ranjbar, R. Sbiaa, and T. C. Chong, J. Vac. Sci. Technol. B **29**, 0110351-0110357 (2011).
[203] R. A. Farrell, N. Kehagias, M. T. Shaw, V. Reboud, M. Zelsmann, J. D. Holmes, C. M. Sotomayor Torres, and M. A. Morris, ACS Nano **5**, 1073–1085 (2011).
[204] S. Darwich, K. Mougin, L. Vidal, E. Gnecco, and H. Haidara, Nanoscale **3**, 1211–1217 (2011).
[205] N. Vogel, J. Fischer, R. Mohammadi, M. Retsch, H. J. Butt, K. Landfester, C. K. Weiss, and M. Kreiter, Nano Lett. **11**, 446–454 (2011).
[206] S. Yang, F. Xu, S. Ostendorp, G. Wilde, H. Zhao, and Y. Lei, Adv. Funct. Mater. **21**, 2446–2455 (2011).
[207] S. Yang, J. Xu, Z. Wang, H. Zeng, and Y. Lei, J. Mater. Chem. **21**, 11930–11935 (2011).
[208] J. Xiao, and L. Qi, Nanoscale **3**, 1383–1396 (2011).
[209] H. Yabu, T. Jinno, K. Koike, T. Higuchi, and M. Shimomura, Macromolecules **44**, 5868–5873 (2011).
[210] Z. C. Chen, M. H. Hong, H. Dong, Y. D. Gong, C. S. Lim, L. P. Shi, and T. C. Chong, Appl. Phys. A **101**, 33–36 (2010).
[211] C. S. Lim, M. H. Hong, Y. Lin, Q. Xie, B. S. Luk'Yanchuk, A. Senthil Kumar, and M. Rahman, Appl. Phys. Lett. **89**, 191125 (2006).
[212] Y. Lin, M. H. Hong, T. C. Chong, C. S. Lim, G. X. Chen, L. S. Tan, Z. B. Wang, and L. P. Shi, Appl. Phys. Lett. **89**, 041108 (2006).
[213] M. C. Gwinner, E. Koroknay, F. Liwei, P. Patoka, W. Kandulski, M. Giersig, and H. Giessen, Small **5**, 400–406 (2009).
[214] S. Cataldo, J. Zhao, F. Neubrech, B. Frank, C. Zhang, P. V. Braun, and H. Giessen, ACS Nano **6**, 979–985 (2012).
[215] C. W. Qiu, A. Novitsky, L. Gao, J. W. Dong, and B. Luk'Yanchuk, arXiv:1202.5613v1 (2012).
[216] M. I. Tribelsky, A. E. Miroshnichenko, and Y. S. Kivshar, Europhys. Lett. **97**, 44005 (2012).
[217] C. L. Garrido Alzar, M. A. G. Martinez, and P. Nussenzveig, Am. J. Phys. **70**, 37–41 (2002).
[218] Y. S. Joe, A. M. Satanin, and C. S. Kim, Phys. Scr. **74**, 259–266 (2006).
[219] E. D. Palik, Handbook of Optical Constants of Solids (Academic, New York, 1985).
[220] M. Rahmani, B. Lukiyanhuk, T. Y. F. Liew, and M. H. Hong, in: Proceedings of Laser Science to Photonic Application (CLEO), San Jose, USA, 2012, paper QTh4F.2.
[221] Y. Cui, J. Zhou, V. A. Tamma, and W. Park, ACS Nano **6**, 2385–2393 (2012).
[222] N. A. Mirin, K. Bao, and P. Nordlander, J. Phys. Chem. A **113**, 4028–4034 (2009).
[223] M. Rahmani, D. Y. Lei, V. Giannini, B. Lukiyanchuk, M. Ranjbar, T. Y. F. Liew, M. H. Hong, and S. A. Maier, Nano Lett. **12**, 2101–2106 (2012).
[224] J. Ye, F. Wen, H. Sobhani, J. B. Lassiter, P. V. Dorpe, P. Nordlander, and N. J. Halas, Nano Lett. **12**, 1660–1667 (2012).
[225] A. L. Koh, A. I. Fernández-Domínguez, D. W. McComb, S. A. Maier, and J. K. W. Yang, Nano Lett. **11**, 1323–1330 (2011).
[226] E. S. Barnard, T. Coenen, E. J. R. Vesseur, A. Polman, and M. L. Brongersma, Nano Lett. **11**, 4265–4269 (2011).
[227] C. E. Hofmann, E. J. R. Vesseur, L. A. Sweatlock, H. J. Lezec, F. J. G. De Abajo, A. Polman, and H. A. Atwater, Nano Lett. **7**, 3612–3617 (2007).
[228] X. Zhu, J. Zhang, J. Xu, H. Li, X. Wu, Z. Liao, Q. Zhao, and D. Yu, ACS Nano **5**, 6546–6552 (2011).
[229] P. S. Carney, B. Deutsch, A. A. Govyadinov, and R. Hillenbrand, ACS Nano **6**, 8–12 (2012).
[230] M. Frimmer, T. Coenen, and A. F. Koenderink, Phys. Rev. Lett. **108**, 077404 (2012).
[231] J. B. Lassiter, H. Sobhani, M. W. Knight, W. S. Mielczarek, P. Nordlander, and N. J. Halas, Nano Lett. **12**, 1058–1062 (2011).
[232] M. Aeschlimann, M. Bauer, D. Bayer, T. Brixner, F. J. García De Abajo, W. Pfeiffer, M. Rohmer, C. Spindler, and F. Steeb, Nature **446**, 301–304 (2007).
[233] J. Fan, C. Wu, K. Bao, R. Bardhan, B. Jiming, V. Manoharan, N. Halas, P. Nordlander, G. Shvets, and F. Capasso, in: Proceedings of Winter Topicals (WTM), IEEE, Keystone, CO, USA, 2012, pp. 53–54.
[234] L. Chuntonov, and G. Haran, Nano Lett. **11**, 2440–2445 (2011).
[235] L. S. Slaughter, Y. Wu, B. A. Willingham, P. Nordlander, and S. Link, ACS Nano **4**, 4657–4666 (2010).
[236] A. J. Mastroianni, S. A. Claridge, and A. Paul Alivisatos, J. Am. Chem. Soc. **131**, 8455–8459 (2009).
[237] J. Zhao, B. Frank, S. Burger, and H. Giessen, ACS Nano **5**, 9009–9016 (2011).
[238] H. Haken, and H. C. Wolf, Molecular Physics and Elements of Quantum Chemistry (Springer, Berlin, 2003).
[239] N. Liu, S. Mukherjee, K. Bao, L. V. Brown, J. Dorfmüller, P. Nordlander, and N. J. Halas, Nano Lett. **12**, 364–369 (2011).
[240] T. J. Davis, M. Hentschel, N. Liu, and H. Giessen, ACS Nano **6**, 1291–1298 (2012).
[241] N. Liu, M. Hentschel, T. Weiss, A. P. Alivisatos, and H. Giessen, Science **332**, 1407–1410 (2011).
[242] R. Taubert, M. Hentschel, J. Kästel, and H. Giessen, Nano Lett. **12**, 1367–1371 (2012).
[243] A. Manjavacas, F. J. G. D. Abajo, and P. Nordlander, Nano Lett. **11**, 2318–2323 (2011).
[244] S. Savasta, R. Saija, A. Ridolfo, O. Di Stefano, P. Denti, and F. Borghese, ACS Nano **4**, 6369–6376 (2010).
[245] K. Tanaka, E. Plum, J. Y. Ou, T. Uchino, and N. I. Zheludev, Phys. Rev. Lett. **105**, 227403 (2010).
[246] X. Wu, S. K. Gray, and M. Pelton, Opt. Express **18**, 23633–23645 (2010).
[247] W. Ding, B. Luk'yanchuk, and C. W. Qiu, Phys. Rev. A **85**, 025806 (2012).
[248] C. Wu, A. B. Khanikaev, R. Adato, N. Arju, A. A. Yanik, H. Altug, and G. Shvets, Nature Mater. **11**, 69–75 (2011).
[249] N. Liu, and A. Pucci, Nature Mater. **11**, 9–10 (2012).
[250] F. Neubrech, A. Pucci, T. W. Cornelius, S. Karim, A. García-Etxarri, and J. Aizpurua, Phys. Rev. Lett. **101**, 157403 (2008).
[251] J. J. Sáenz, Nature Photon. **5**, 514–515 (2011).
[252] J. Chen, J. Ng, Z. Lin, and C. T. Chan, Nature Photon. **5**, 531–534 (2011).
[253] M. Aeschlimann, T. Brixner, A. Fischer, C. Kramer, P. Melchior, W. Pfeiffer, C. Schneider, C. Strüber, P. Tuchscherer, and D. V. Voronine, Science **333**, 1723–1726 (2011).
[254] T. Brixner, and G. Gerber, Opt. Lett. **26**, 557–559 (2001).
[255] N. Yu, P. Genevet, M. A. Kats, F. Aieta, J. P. Tetienne, F. Capasso, and Z. Gaburro, Science **334**, 333–337 (2011).
[256] P. Spinelli, M. Hebbink, R. De Waele, L. Black, F. Lenzmann, and A. Polman, Nano Lett. **11**, 1760–1765 (2011).

[257] A. Tittl, P. Mai, R. Taubert, D. Dregely, N. Liu, and H. Giessen, Nano Lett. **11**, 4366–4369 (2011).
[258] V. I. Belotelov, I. A. Akimov, M. Pohl, A. N. Kalish, S. Kasture, A. S. Vengurlekar, A. V. Gopal, V. A. Kotov, D. Yakovlev, A. K. Zvezdin, and M. Bayer, J. Phys. Conf. Ser. **303**, 012038 (2011).
[259] V. I. Belotelov, I. A. Akimov, M. Pohl, V. A. Kotov, S. Kasture, A. S. Vengurlekar, A. V. Gopal, D. R. Yakovlev, A. K. Zvezdin, and M. Bayer, Nature Nanotechnol. **6**, 370–376 (2011).
[260] V. P. Zharov, Nature Photon. **5**, 110–116 (2011).
[261] P. Genevet, J. P. Tetienne, E. Gatzogiannis, R. Blanchard, M. A. Kats, M. O. Scully, and F. Capasso, Nano Lett. **10**, 4880–4883 (2010).
[262] K. Lodewijks, W. Van Roy, G. Borghs, L. Lagae, and P. Van Dorpe, Nano Lett. **12**, 1655–1659 (2012).
[263] E. Loginov, L. F. Gomez, N. Chiang, A. Halder, N. Guggemos, V. V. Kresin, and A. F. Vilesov, Phys. Rev. Lett. **106**, 233401 (2011).